



35 <sup>16</sup>Sorbonne Universités, UPMC, Univ Paris 06, CNRS, EPHE, UMR 7619 METIS,  
36 Paris, France  
37 <sup>17</sup>Department of Forest Sciences, University of Helsinki, Finland  
38 <sup>18</sup>Université d'Orléans / CNRS /BRGM, ISTO, UMR 7327, Orléans, France  
39 <sup>19</sup>Department of Biology, University of Turku, Finland  
40 <sup>20</sup>York Institute for Tropical Ecosystems, Environment Department, Wentworth Way  
41 University of York, York, UK  
42 <sup>21</sup>Department of Geography, Durham University, Durham, UK  
43 <sup>22</sup>Departamento de Edafología e Química Agrícola, Universidade de Santiago de  
44 Compostela, Santiago de Compostela, Spain  
45 <sup>23</sup>Division of Marine Geology & Geophysics, University of Miami – RSMAS, Miami,  
46 USA  
47 <sup>24</sup>Department of Chemistry, Claflin University, Orangeburg, USA  
48 <sup>25</sup>Peatland Ecology Research Group (PERG), Centre for Northern Studies, Université  
49 Laval, Quebec City, Canada  
50 <sup>26</sup>Department of Soil Science, University of São Paulo, Piracicaba, Brazil

51

52 \*Corresponding author ([david.naafs@bristol.ac.uk](mailto:david.naafs@bristol.ac.uk))

53

## 54 **Abstract**

55 Glycerol dialkyl glycerol tetraethers (GDGTs) are membrane-spanning lipids from  
56 Bacteria and Archaea that are ubiquitous in a range of natural archives and especially  
57 abundant in peat. Previous work demonstrated that the distribution of bacterial  
58 branched GDGTs (brGDGTs) in mineral soils is correlated to environmental factors  
59 such as mean annual air temperature (MAAT) and soil pH. However, the influence of  
60 these parameters on brGDGT distributions in peat is largely unknown. Here we  
61 investigate the distribution of brGDGTs in 470 samples from 96 peatlands around the  
62 world with a broad mean annual air temperature (−8 to 27 °C) and pH (3–8) range and  
63 present the first peat-specific brGDGT-based temperature and pH calibrations. Our  
64 results demonstrate that the degree of cyclisation of brGDGTs in peat is positively  
65 correlated with pH,  $\text{pH} = 2.49 \times \text{CBT}_{\text{peat}} + 8.07$  ( $n = 51$ ,  $R^2 = 0.58$ ,  $\text{RMSE} = 0.8$ ) and  
66 the degree of methylation of brGDGTs is positively correlated with MAAT,  
67  $\text{MAAT}_{\text{peat}} (\text{°C}) = 52.18 \times \text{MBT}_{5\text{me}'} - 23.05$  ( $n = 96$ ,  $R^2 = 0.76$ ,  $\text{RMSE} = 4.7 \text{ °C}$ ).

68 These peat-specific calibrations are distinct from the available mineral soil  
69 calibrations. In light of the error in the temperature calibration ( $\sim 4.7$  °C), we urge  
70 caution in any application to reconstruct late Holocene climate variability, where the  
71 climatic signals are relatively small, and the duration of excursions could be brief.  
72 Instead, these proxies are well-suited to reconstruct large amplitude, longer-term  
73 shifts in climate such as deglacial transitions. Indeed, when applied to a peat deposit  
74 spanning the late glacial period ( $\sim 15.2$  kyr), we demonstrate that  $MAAT_{\text{peat}}$  yields  
75 absolute temperatures and relative temperature changes that are consistent with those  
76 from other proxies. In addition, the application of  $MAAT_{\text{peat}}$  to fossil peat (i.e.  
77 lignites) has the potential to reconstruct terrestrial climate during the Cenozoic. We  
78 conclude that there is clear potential to use brGDGTs in peats and lignites to  
79 reconstruct past terrestrial climate.

80

81 *Keyword: GDGT, biomarker, peatland, calibration, lignite*

82

83 Highlights:

- 84 - Analysis of brGDGT distributions in global peat dataset
- 85 - Correlation of brGDGT distributions with peat pH and mean annual air temperature
- 86 - Development of peat-specific temperature and pH proxies

## 87 **1. Introduction**

88 Although reconstructions of terrestrial environments are crucial for the understanding  
89 of Earth's climate system, suitable depositional archives (especially longer continuous  
90 sequences) are rare on land. Peatlands and lignites (naturally compressed ancient peat)  
91 are one exception and offer remarkable preservation of organic matter. Peats can be  
92 found in all climate zones where suitable waterlogged conditions exist. Typical peat  
93 accumulation rates are on the order of 1-2 mm/year (Gorham et al., 2003) and because  
94 they exhibit minimal bioturbation (although roots might be present) they are widely  
95 used as climate archives during the late Quaternary, predominantly the Holocene  
96 (e.g., Barber, 1993; Chambers and Charman, 2004). Peat-based proxies include those  
97 based on plant macrofossils, pollen, and testate amoebae (e.g., Woillard, 1978;  
98 Mauquoy et al., 2008; Väliranta et al., 2012), inorganic geochemistry (e.g., Burrows  
99 et al., 2014; Chambers et al., 2014; Hansson et al., 2015; Vanneste et al., 2015), (bulk)  
100 isotope signatures (e.g., Cristea et al., 2014; Roland et al., 2015) and organic  
101 biomarkers (e.g., Nichols et al., 2006; Pancost et al., 2007; Pancost et al., 2011;  
102 Huguet et al., 2014; Zocatelli et al., 2014; Schellekens et al., 2015; Zheng et al.,  
103 2015). Although these proxies can be used to provide a detailed reconstruction of the  
104 environment and biogeochemistry within the peat during deposition, an accurate  
105 temperature or pH proxy for peat is currently lacking (Chambers et al., 2012). This is  
106 particularly problematic because temperature and pH are key environmental  
107 parameters that directly affect vegetation type, respiration rates, and a range of other  
108 wetland features (e.g., Lafleur et al., 2005; Yvon-Durocher et al., 2014). The aim of  
109 this paper is to develop peat-specific pH and temperature proxies for application to  
110 peat cores as well as ancient peats from the geological record preserved as lignites.

111 We focus on using membrane-spanning glycerol dialkyl glycerol tetraether  
112 (GDGT) lipids. In general, two types of GDGTs are abundant in natural archives such  
113 as peats: 1) isoprenoidal (iso)GDGTs with *sn*-1 glycerol stereochemistry that are  
114 synthesized by a wide range of Archaea, and 2) branched (br)GDGTs with *sn*-3  
115 glycerol stereochemistry that are produced by Bacteria (see review by Schouten et al.,  
116 2013 and references therein). A wide range of brGDGTs occur in natural archives  
117 such as mineral soils and peat; specifically, tetra-, penta-, and hexamethylated  
118 brGDGTs, each of which can contain 0, 1, or 2 cyclopentane rings (Weijers et al.,  
119 2006b). In addition, recent studies using peat and mineral soils have demonstrated that  
120 the additional methyl group(s) present in penta- and hexamethylated brGDGTs can

121 occur on either the  $\alpha$  and/or  $\omega$ -5 position (5-methyl brGDGTs) or the  $\alpha$  and/or  $\omega$ -6  
122 position (6-methyl brGDGTs) (De Jonge et al., 2013; De Jonge et al., 2014).

123 brGDGTs are especially abundant in peat, in fact brGDGTs were first  
124 discovered in a Dutch peat (Sinninghe Damsté et al., 2000). The concentration of  
125 brGDGTs (as well as isoGDGTs) is much higher in the water saturated and  
126 permanently anoxic catotelm of peat compared to the predominantly oxic acrotelm,  
127 suggesting that brGDGTs are produced by anaerobic bacteria (Weijers et al., 2004;  
128 Weijers et al., 2006a; Weijers et al., 2011), potentially members of the phylum  
129 *Acidobacteria* (Weijers et al., 2009; Sinninghe Damsté et al., 2011; Sinninghe Damsté  
130 et al., 2014). Although the exact source organism(s) are/is currently unknown, in  
131 mineral soils (and potentially lakes) the distribution of bacterial brGDGTs is  
132 correlated with mean annual air temperature (MAAT) and pH (Weijers et al., 2007;  
133 Peterse et al., 2012; De Jonge et al., 2014; Loomis et al., 2014; Li et al., 2016). Over  
134 the past decade ancient deposits of mineral soils (e.g., Peterse et al., 2014) and peat  
135 (e.g., Ballantyne et al., 2010) have been used to reconstruct past terrestrial  
136 temperatures.

137 Mineral soils differ from peat as the latter are normally water saturated,  
138 consist predominantly of (partially decomposed) organic matter (the organic carbon  
139 content of peat is typically > 30 wt.%), are typically acidic (pH 3-6), and have much  
140 lower density. The combination of these factors means that peat becomes anoxic at  
141 relatively shallow depths, whereas mineral soils are typically oxic. Indeed, Loomis et  
142 al. (2011) showed that the brGDGT distribution in waterlogged soils is different from  
143 that in dry soils and Dang et al. (2016) recently provided direct evidence of moisture  
144 control on brGDGT distributions in soils. These differences suggest that microbial  
145 lipids in peat might not reflect environmental variables, i.e. pH and temperature, in  
146 the same way as they do in mineral soils.

147 Despite the high concentration of GDGTs in peats relatively few studies have  
148 examined the environmental controls on their distribution in such settings (Huguet et  
149 al., 2010; Weijers et al., 2011; Huguet et al., 2013; Zheng et al., 2015). Those studies  
150 found that the application of soil-based proxies to peats can result in unrealistically  
151 high temperature and pH estimates compared to the instrumental record. However,  
152 owing to the small number of peats that have been studied to date as well as the lack  
153 of peatland diversity sampled (the majority of peats sampled for these studies come  
154 from temperate climates in Western Europe), the correlation of temperature and pH

155 with brGDGT distribution in peats is poorly constrained. Notably, the lack of tropical  
156 peat brGDGT studies limits interpretations of brGDGT distributions in lignite  
157 deposits from past greenhouse climates (Weijers et al., 2011).

158 Here we compare brGDGT distributions in a newly generated global data set  
159 of peat with MAAT and (where available) *in situ* peat pH measurements. Our aim is  
160 to gain an understanding of the impact of these environmental factors on the  
161 distribution of brGDGTs in peat and develop for the first time peat-specific  
162 temperature and pH proxies that can be used to reconstruct past terrestrial climate.

163

## 164 **2. Material and methods**

### 165 *2.1 Peat material*

166 We generated a collection of peat comprising a diverse range of samples from around  
167 the world (Fig. 1). In total, our database consists of 470 samples from 96 different  
168 peatlands. In order to assess the variation in brGDGT distribution within one location,  
169 where possible we determined the brGDGT distribution in multiple horizons from  
170 within the top 1m of peat (typically representing several centuries of accumulation)  
171 and/or analyzed samples taken at slightly different places within the same peatland. A  
172 peat deposit typically consists of an acrotelm and catotelm, although marked  
173 heterogeneity can exist even over short distances (Baird et al., 2016). The acrotelm is  
174 located above the water table for most of the year and characterized by oxic  
175 conditions and active decomposition. The acrotelm overlies the catotelm, which is  
176 permanently waterlogged and characterized by anoxic conditions and very slow  
177 decomposition. Our dataset spans those biogeochemical gradients (e.g. acro/catotelm).  
178 Variations in peat accumulation rates differ between sites, implying that the ages of  
179 the brGDGT-pool might differ.

180 Our database includes peats from six continents and all major climate zones,  
181 ranging from high latitude peats in Siberia, Canada, and Scandinavia to tropical peats  
182 in Indonesia, Africa, and Peru (Fig. 2). It covers a broad range in MAAT from -8 to  
183 27 °C. Although most samples come from acidic peats with pH <6, the dataset  
184 includes several alkaline peats and overall our dataset spans a pH range from 3 to 8.  
185 All samples come from freshwater peatlands, except for the one from the Shark River  
186 peat (Everglades, USA) that is marine influenced. Unsurprisingly, given their global  
187 distribution, the peats are characterized by a wide variety of vegetation, ranging from

188 *Sphagnum*-dominated ombrotrophic peats that are abundant in high-latitude and  
189 temperate climates to (sub)tropical peats dominated by vegetation such as *Sagittaria*  
190 (arrowhead) and *Cyperaceae* (sedge), and forested tropical peatlands.

191

## 192 2.2 Environmental parameters

193 The distribution of brGDGTs was compared to MAAT and *in situ* pH. MAAT was  
194 obtained using the simple bioclimatic model PeatStash, which provides surface air  
195 temperatures globally with a 0.5 degree spatial resolution (for details, see Kaplan et  
196 al., 2003; Gallego-Sala and Prentice, 2013). The temperature data in PeatStash is  
197 obtained by interpolating long-term mean weather station climatology (temperature,  
198 precipitation and the fraction of possible sunshine hours) from around the world for  
199 the period 1931–1960 (Climate 2.2 data are available online [http://www.pik-](http://www.pik-potsdam.de/~cramer/climate.html)  
200 [potsdam.de/~cramer/climate.html](http://www.pik-potsdam.de/~cramer/climate.html)). Crucially, mean annual temperatures in peat are  
201 similar to MAAT, assuming that the peat is not snow-covered for long periods of time  
202 (McKenzie et al., 2007; Weijers et al., 2011). The temperature at the top surface of  
203 (high-latitude) peat can differ from the MAAT due to insolation by snow during  
204 winter and intense heating during summer. Despite this, the seasonal temperature  
205 fluctuations in peat are dampened at depth as temperatures converge to MAAT  
206 (Hillel, 1982; Laiho, 2006; McKenzie et al., 2007; Weijers et al., 2011). We assume  
207 that all peat horizons experienced MAAT (the only data available on a global basis).  
208 This is likely an oversimplification that introduces some additional uncertainty in our  
209 calibration.

210 Where available, pH data were obtained from measured values reported in the  
211 literature or our measurements during sampling. For peats, pH cannot be determined  
212 using dried material, as is normally done for soils (Stanek, 1973). Accurate pH  
213 measurements can only be obtained from *in situ* measurements, especially for  
214 groundwater-fed wetlands, and these are not available for all locations.

215

## 216 2.3 Lipid extraction

217 For the majority of samples (>430 out of 470), between 0.1 and 0.5 g of dried bulk  
218 peat were extracted with an Ethos Ex microwave extraction system with 20 mL of a  
219 mixture of dichloromethane (DCM) and methanol (MeOH) (9:1, v/v) at the Organic  
220 Geochemistry Unit (OGU) in Bristol. The microwave program consisted of a 10 min  
221 ramp to 70 °C (1000 W), 10 min hold at 70 °C (1000 W), and 20 min cool down.

222 Samples were centrifuged at 1700 rounds per minute for 3 to 5 min and the  
223 supernatant was removed and collected. 10 mL of DCM:MeOH (9:1) were added to  
224 the remaining peat material and centrifuged again after which the supernatant was  
225 removed and combined with the previously obtained supernatant. This process was  
226 repeated 3 to 6 times, depending on the amount of extracted material, to ensure that  
227 all extractable lipids were retrieved. The total lipid extract (TLE) was then  
228 concentrated using rota-evaporation. An aliquot of the TLE (typically 25%) was  
229 washed through a short (<2 cm) silica column using DCM:MeOH (9:1) to remove any  
230 remaining peat particles. The TLE was dried under a gentle nitrogen flow and then re-  
231 dissolved in hexane/*iso*-propanol (99:1, v/v) and filtered using 0.45 µm PTFE filters.

232 A small number of peats were extracted using different methods and either the  
233 TLE or polar fraction was analyzed for GDGTs (see Table S1). Samples from the  
234 Kyambangunguru peat in Tanzania were extracted using the Bligh-Dyer protocol.  
235 Previous work on peat demonstrated that the brGDGT distribution is similar using  
236 Bligh-Dyer extraction as Soxhlet extraction (Chaves Torres and Pancost, 2016). The  
237 TLE was cleaned over a short Si column at the OGU in Bristol. Both cleaned TLE  
238 and polar fractions were re-dissolved in hexane/*iso*-propanol (99:1, v/v) and filtered  
239 using 0.45 µm PTFE filters.

240

#### 241 2.4 Analytical methods

242 All samples were analyzed for their core lipid GDGT distribution by high  
243 performance liquid chromatography/atmospheric pressure chemical ionisation – mass  
244 spectrometry (HPLC/APCI-MS) using a ThermoFisher Scientific Accela Quantum  
245 Access triplequadrupole MS. Normal phase separation was achieved using two ultra-  
246 high performance liquid chromatography silica columns, following Hopmans et al.  
247 (2016). Crucially this method allows for the separation of the 5- and 6-methyl  
248 brGDGT isomers. Injection volume was 15 µL, typically from 100 µL. Analyses were  
249 performed using selective ion monitoring mode (SIM) to increase sensitivity and  
250 reproducibility ( $m/z$  1302, 1300, 1298, 1296, 1294, 1292, 1050, 1048, 1046, 1036,  
251 1034, 1032, 1022, 1020, 1018, 744, and 653). The results were integrated manually  
252 using the Xcalibur software. Based on daily measurements of an in-house generated  
253 peat standard, analytical precession ( $\sigma$ ) over the 12 months during which the data  
254 were analyzed is 0.01 for the proxy index we define below ( $MBT_{5me}$ , eq. 2).

255

256 2.5 Proxy calculation

257 Guided by previous studies we used a range of proxies to express ratios of different  
 258 GDGTs and the nomenclature of De Jonge et al. (2014) (Fig. 1).

259

eq. (1) MBT

$$= \frac{(Ia + Ib + Ic)}{(Ia + Ib + Ic + IIa + IIa' + IIb + IIb' + IIc + IIc' + IIIa + IIIa' + IIIb + IIIb' + IIIc + IIIc')}$$

260 The original methylation of branched tetraether (MBT) index compared the relative  
 261 abundance of tetramethylated brGDGTs (compounds Ia-Ic) to that of penta-  
 262 (compounds IIa-IIc') and hexamethylated (compounds IIIa-IIIc') brGDGTs that have  
 263 one or two additional methyl groups (Weijers et al., 2007). It was recently discovered  
 264 that the additional methyl groups in penta- and hexamethylated brGDGTs can also  
 265 occur at the C6 position (6-methyl brGDGTs, indicated by a prime symbol; e.g.  
 266 brGDGT-IIa'): the 6-methyl penta- and hexamethylated brGDGTs (De Jonge et al.,  
 267 2013). Excluding the 6-methyl brGDGTs from the MBT index resulted in the  
 268 MBT<sub>5me'</sub> index. In the global soil database the application of MBT<sub>5me'</sub> led to an  
 269 improved correlation with temperature (De Jonge et al., 2014).

eq. (2)  $MBT'_{5ME} = \frac{(Ia + Ib + Ic)}{(Ia + Ib + Ic + IIa + IIb + IIc + IIIa)}$

270 In addition to different number of methyl groups, brGDGTs can contain up to two  
 271 cyclopentane moieties (e.g., brGDGT-Ib and -Ic). CBT' is a modified version of the  
 272 original cyclisation of branched tetraether (CBT) index (Weijers et al., 2007) and in  
 273 soils CBT' has the best correlation with pH (De Jonge et al., 2014):

$$eq. (3) CBT' = \log\left(\frac{Ic + IIa' + IIb' + IIc' + IIIa' + IIIb' + IIIc'}{Ia + IIa + IIIa}\right)$$

274 The isomer ratio of 6-methyl brGDGTs (IR<sub>6me</sub>) reflects the ratio between 5- and 6-  
 275 methyl brGDGTs (Yang et al., 2015) with low (high) values indicative of a  
 276 dominance of 5-methyl (6-methyl) brGDGTs:

eq. (4)  $IR_{6me} = \left(\frac{IIa' + IIb' + IIc' + IIIa' + IIIb' + IIIc'}{IIa + IIa' + IIb + IIb' + IIc + IIc' + IIIa + IIIa' + IIIb + IIIb' + IIIc + IIIc'}\right)$

277

278 The isomerization of branched tetraethers (IBT) is related to IR<sub>6me</sub> but reflects the  
 279 isomerization of brGDGT-IIa and -IIIa only (Ding et al., 2015):

$$eq. (5) IBT = -\log\left(\frac{IIa' + IIIa'}{IIa + IIIa}\right)$$

280 The branched versus isoprenoidal tetraether (BIT) index (Hopmans et al., 2004)  
 281 reflects the relative abundance of the major bacterial brGDGTs versus a specific  
 282 archaeal isoGDGT, crenarchaeol (Fig. 1), produced by *Thaumarchaeota* (Sinninghe  
 283 Damsté et al., 2002):

$$eq. (6) BIT = \frac{Ia + IIa + IIa' + IIIa + IIIa'}{Ia + IIa + IIa' + IIIa + IIIa' + cren.}$$

284 Finally, the isoprenoidal over branched GDGT ratio ( $R_{i/b}$ ), related to the BIT index,  
 285 records the relative abundance of archaeal isoGDGTs over bacterial brGDGTs (Xie et  
 286 al., 2012).

$$eq. (7) R_{i/b} = \frac{\sum isoGDGTs}{\sum brGDGTs}$$

287

## 288 2.6 Statistical methods

289 Temperature and pH calibrations were obtained using the average proxy value for  
 290 each peat and Deming regressions. The software we used was RStudio  
 291 (RStudio Team, 2015) and Method Comparison Regression (MCR) package  
 292 (Manuilova et al., 2014), which are freely available to download<sup>1</sup>. The Rscript and  
 293 data are available in the appendices.

294 Deming regressions differ from simple linear regression, which so far have  
 295 been used in brGDGT proxy calibrations, as they account for error in the data on both  
 296 the x- (e.g., proxy) and y-axis (e.g., environmental variable) (Adcock, 1878).  
 297 We used the average proxy value for each peat to calculate Deming regressions,  
 298 calibration errors (RMSE, see below), and calibration coefficients of determination  
 299 ( $R^2$ ). The errors associated with proxy measurements (e.g.  $MBT_{5me}'$ ) and  
 300 environmental parameters (MAAT/pH) are independent and assumed to be normally  
 301 distributed. To calculate a Deming regression, the ratio of variances ( $\delta$ ) must be  
 302 calculated. For MAAT we took a standard deviation ( $\sigma$ ) of 1.5 °C based on the  
 303 estimated mean predictive error of up to 1.4 °C for mean temperature in a similar  
 304 dataset (New et al., 1999). For pH we took a standard deviation of 0.5 based on the  
 305 average reported heterogeneity in pH for the peatlands used in the database (see  
 306 Supplementary Table 1). For  $MBT_{5me}'$ ,  $CBT'$ , and  $CBT_{peat}$  we calculated the average

<sup>1</sup> <https://www.rstudio.com> and <https://cran.r-project.org/web/packages/mcr/index.html>

307 standard deviation of each proxy from the entire peat data set (0.05, 0.25, and 0.2,  
 308 respectively). This results in a ratio of variances of 0.0011 for the MBT<sub>5me</sub>'/MAAT  
 309 calibration and 0.25 and 0.16 for the pH calibration based on CBT' and CBT<sub>peat</sub>,  
 310 respectively. Residuals were calculated for the full dataset and using

$$eq. (8) \text{ Residual}_y = y_{observed} - y_{predicted}$$

311 The root mean square error (RMSE) for  $y$ , the predictive error for the  
 312 environmental parameter of interest (MAAT or pH), was calculated for the average  
 313 proxy value of each peat and using

$$eq. (9) RSME_y = \sqrt{\frac{\sum_{x=1}^n (y_{x,observed} - y_{x,predicted})^2}{n}} \times \frac{n}{df}$$

314 Where  $df$  stands for degrees of freedom, which in this case is  $n-1$ .

315

### 316 **3. Results**

317 Although we did not calculate concentrations, based on changes in signal intensity the  
 318 relative abundance of GDGTs was always higher at depth compared to the top (~0–  
 319 20) cm of peat. BIT indices (eq. 6) range between 0.75 and 1, but 99% of the samples  
 320 have a BIT value  $\geq 0.95$ . Similarly,  $R_{i/b}$  ratios are typically  $< 0.5$ . Only three samples  
 321 from the São João da Chapada peat in Brazil have a  $R_{i/b}$  ratio  $> 1$ .

322 The majority of brGDGTs are tetramethylated and 5-methyl penta- and  
 323 hexamethylated brGDGTs. The most abundant brGDGTs in peat are brGDGT-Ia and  
 324 IIa. By extension, the IR<sub>6me</sub> ratio (eq. 4) is low. brGDGTs containing cyclopentane  
 325 moieties are much less abundant than acyclic brGDGTs and brGDGT-IIIb(?) and -  
 326 IIIc(?) are either below detection limit or present at trace abundances ( $\leq 1\%$  of total  
 327 brGDGTs). Indeed, three brGDGTs dominate the entire global dataset: tropical peats  
 328 contain almost exclusively brGDGT-Ia (up to 99% of total brGDGTs), whereas in  
 329 high-latitude peats brGDGT-IIa and -IIIa are dominant (Fig. 3).

330

### 331 **4. Discussion**

332 The observation that  $R_{i/b}$  ratios are low in most peats is consistent with previous  
 333 observations that bacterial brGDGTs dominate over archaeal isoprenoidal GDGTs in  
 334 peat (Schouten et al., 2000; Sinninghe Damsté et al., 2000; Pancost et al., 2003) and  
 335 mineral soils (Hopmans et al., 2004).

336

#### 337 *4.1 Shallow vs deep GDGT distributions*

338 The apparent increase in GDGT abundance with depth is consistent with previous  
339 observations in peatlands (Weijers et al., 2004; Peterse et al., 2011) and reflects the  
340 combined effects of preferential GDGT production in anaerobic settings and the  
341 accumulation of fossil GDGTs over time at depth (Liu et al., 2010; Weijers et al.,  
342 2011).

343 In one high-latitude peat (Saxnäs Mosse, Sweden) the distribution of both  
344 intact polar lipids (compounds still containing a polar head groups) and core  
345 brGDGTs (compounds having lost their polar head group) differed between the acro-  
346 and catotelm and brGDGT abundances were much higher in the latter (Weijers et al.,  
347 2009; Peterse et al., 2011). Based on these results Peterse et al. (2011) speculated that  
348 microbial communities differed between the oxic acrotelm and anoxic catotelm. As  
349 oxygen content can influence cellular lipid composition of bacteria, Huguet et al.  
350 (2010) speculated that oxygen availability could be one of the factors directly  
351 influencing the brGDGT synthesis by bacteria in peat, as opposed to influencing the  
352 type of source organism(s). Studies from lakes also suggested that changes in lake  
353 oxygenation state can influence the brGDGT distribution (Tierney et al., 2012;  
354 Loomis et al., 2014).

355 Our dataset consists of a mixture of surface (0–15 cm) and deeper samples  
356 that extend through the top one meter of peat. For the majority of peats there is no  
357 detailed information available on water table depths and location of the acro/catotelm  
358 boundary. Nonetheless, to provide a first order assessment on whether there is a  
359 systematic and significant difference in core brGDGT distribution between the upper  
360 (assumed to be generally oxic) and underlying anoxic peat, we compared the relative  
361 abundance of the three most abundant brGDGTs (Ia, IIa, and IIIa) in the shallow  
362 surface peat (top 15 cm) with that of the deep peat below 15 cm (Fig. 3), although we  
363 acknowledge that this is likely an oversimplification.

364 There are some differences. In general the relative abundance of brGDGT-Ia  
365 is slightly higher in the top 15 cm of a peat compared to the peat below 15 cm,  
366 especially when its abundance is < 60%. Overall, however, the distributions plot  
367 along the 1:1 line, indicating that there is no systematic difference in brGDGT  
368 distribution between the (assumed) oxic surface and the peat below 15 cm (likely  
369 anoxic). This does not preclude differences in brGDGT production between oxic and  
370 anoxic conditions, but this appears to be primarily expressed via greater production of

371 brGDGTs under anoxic conditions as demonstrated by the higher abundance of  
372 GDGTs across the acro/catotelm boundary (Weijers et al., 2006a). These results  
373 provide indirect evidence that oxygen availability does not significantly impact the  
374 degree of methylation of (core) brGDGTs. One possible explanation for why oxygen  
375 availability does not affect distributions is that brGDGTs could be predominantly  
376 produced by anaerobes throughout the peat, in low abundance in anaerobic  
377 microenvironments in shallow peat and in high abundance in the anaerobic catotelm.

378 Several (high-latitude) peats, however, do appear to exhibit strong variations  
379 between deep and shallow sections of the peat. The down core records from Stordalen  
380 (Sweden) and Andorra (S. Patagonia), for example, are characterized by a large and  
381 abrupt shift in brGDGT distribution at depth (Fig. 4). The  $MBT_{5me}'$  indices recorded  
382 at the very top of these high-latitude peats are between 0.8 and 0.6, as high as those  
383 found in mid-latitude and subtropical peats, but decrease to values between 0.2 and  
384 0.4 below ~30 cm. Peats from temperate climates (e.g. Walton moss, UK) and the  
385 tropics (e.g. Sebangau, Indonesia) display much smaller or no change in brGDGT  
386 distribution with depth (Fig. 4 and 5). It appears that this offset in brGDGT  
387 distribution with depth is amplified in high-latitude peats. This is consistent with  
388 previous studies that indicated a difference in brGDGT-distribution between the acro-  
389 and catotelm in a high-latitude peat from southern Sweden (Weijers et al., 2009;  
390 Peterse et al., 2011).

391 We argue that the high  $MBT_{5me}'$  values at the top of these high-latitude peats  
392 are heavily biased towards summer temperatures. At these settings winter  
393 temperatures are often below freezing for a prolonged period, likely causing bacterial  
394 growth and GDGT production to slow down significantly. Summer temperatures are  
395 much higher (e.g. mean warmest month temperature at Stordalen is around 13 °C), in-  
396 line with the observed relatively high  $MBT_{5me}'$  values (e.g., 0.6-0.7 at Stordalen, see  
397 Figure 4). Deeper in the peat, seasonal temperature fluctuations are much less  
398 pronounced and temperatures rapidly converge to the MAAT (Vitt et al., 1995; Laiho,  
399 2006; McKenzie et al., 2007; Weijers et al., 2011), likely accounting for the lower  
400  $MBT_{5me}'$  values in the deeper peat horizons. Moreover, the greater production of  
401 GDGTs in the anaerobic part of the peat will cause GDGT-based temperatures to  
402 rapidly converge on the deep peat growth temperature, overprinting the seasonal  
403 summer bias of fossil GDGTs synthesized at the surface.

404 This effect is diminished in temperate and especially tropical peatlands from  
405 around sea level, which we attribute to the lack of a preferred growing season in  
406 settings with smaller seasonal temperature ranges. In such settings temperatures are  
407 less frequently (or never) below freezing and brGDGT production in the top of the  
408 peat likely occurs for all or most of the year, such that GDGTs produced in both the  
409 shallow and deeper part of the peat record MAAT. This hypothesis needs further  
410 testing but indicates that 1) brGDGT production may be biased towards the warm  
411 season in the upper part of high-latitude/altitude peats; 2) care has to be taken when  
412 interpreting brGDGT-based trends in the top of such peats; and 3) the temperature  
413 signal in such peats is imparted at depth, such that downcore GDGT variations in  
414 ancient peat archives could potentially be temporally offset (precede) the climate  
415 events that caused them. However, as brGDGTs in long peat cores, and by extension  
416 ancient lignites (fossilized peats), are dominated by production at depth where  
417 temperature equals MAAT (see section 2.2) it is very unlikely that temperatures  
418 obtained from these archives are seasonally biased.

419 In the remainder of this work, for high-latitude peats that show a clear offset  
420 between the top and deeper part of the peat we use only the average GDGT  
421 distribution from below 20 cm, as the majority of change appears to occur in the top  
422 20 cm. For the other peats we retain all data from the upper 1 m, not differentiating  
423 between the acro- and catotelm. To generate the temperature and pH calibrations we  
424 use the average brGDGT distribution for each peatland. For peats where multiple  
425 samples were analyzed, error bars indicate the deviation ( $1 \sigma$ ) from the average.

426

#### 427 *4.2 Influence of temperature and pH on brGDGTs in peats*

428 It is well established that in soils and lakes, environmental conditions such as  
429 temperature and pH are highly correlated with the brGDGT distribution (e.g., Weijers  
430 et al., 2007; Peterse et al., 2012; Schoon et al., 2013; De Jonge et al., 2014; Loomis et  
431 al., 2014; Xiao et al., 2015; Li et al., 2016). In the following sections we investigate  
432 the influence of these parameters on the brGDGT distribution in peat using the  
433 average proxy value (e.g.  $MBT_{5me}$ ) for each peatland.

434

##### 435 *4.2.1 Influence of peat pH on brGDGT distribution*

436 Weijers et al. (2007) demonstrated that in a global mineral soil database the degree of  
437 cyclisation of brGDGTs is correlated to pH, with a higher fractional abundance of

438 brGDGTs that contain cyclopentane moieties in soils with a higher pH. Following the  
439 discovery of 6-methyl brGDGTs (De Jonge et al., 2013), it was shown that the degree  
440 of isomerization of brGDGTs, the ratio of 6-methyl versus 5-methyl brGDGTs, is also  
441 correlated to soil pH, with a higher fractional abundance of 6-methyl brGDGTs in  
442 soils with a higher pH (De Jonge et al., 2014; Xiao et al., 2015). Owing to the limited  
443 pH range of the few peats used to study brGDGTs so far and because all of these  
444 studies pre-date the recent analytical advances that allow for the separation of 5- and  
445 6-methyl brGDGTs, it is unknown whether pH has an influence on brGDGTs in peats  
446 or whether the dependence is similar to that found in soils. Our peat database spans a  
447 pH range from 3 to 8, similar to that of the soil database, allowing us to assess the  
448 influence of pH on the brGDGT distribution in such settings.

449         Although pH measurements are only available in 51 out of 96 peats, our  
450 results indicate that 6-methyl brGDGTs are present at either only trace abundances  
451 ( $IR_{6me} < 0.1$ ) or are absent in acidic peats with  $pH < 5.4$  (Fig 6). Higher ratios occur in  
452 peats with higher pH. The highest ratio (0.58) occurs in the marine-influenced  
453 alkaline peat from the Everglades. Not surprisingly, the fractional abundances of the  
454 three most common 6-methyl brGDGTs (brGDGT-IIa', -IIb', -IIIa') are significantly  
455 correlated with pH with R-values between 0.4 and 0.6 ( $p < 0.01$ ) (Fig. 7). These results  
456 are consistent with observations from soils that indicate a positive correlation between  
457 the fractional abundance of 6-methyl brGDGTs and pH (De Jonge et al., 2014; Xiao  
458 et al., 2015).

459         As a result, the  $IR_{6me}$  as well as the related IBT index, both of which have  
460 been used to reconstruct pH in soils (Ding et al., 2015; Xiao et al., 2015), are  
461 correlated with pH in the peats (not shown). However, this comparison is complicated  
462 by the fact that 6-methyl brGDGTs are absent in many of the peats. For  $IR_{6me}$  the  
463 absence of 6-methyl brGDGTs results in values that are 0, whereas IBT cannot be  
464 calculated for samples that lack 6-methyl brGDGTs as the logarithm of zero is  
465 undefined.

466         The abundance of 6-methyl brGDGTs is generally lower in peats than in  
467 mineral soils with comparable pH. Indeed, 6-methyl brGDGTs are present in 99% of  
468 all soils in the global soil database, including soils with  $pH < 5$  where  $IR_{6me}$  ratios can  
469 be as high as 0.4 (Fig. 6). Recent work has shown that in addition to pH the fractional  
470 abundance of 6-methyl brGDGTs is negatively correlated with soil water content,  
471 with fewer 6-methyl brGDGTs versus 5-methyl brGDGTs in soils with 60% water

472 content compared to soils with < 10% water content (Dang et al., 2016). It is likely  
 473 that the negative correlation between soil water content and fractional abundance of 6-  
 474 methyl brGDGTs can explain the overall lower IR<sub>6me</sub> in peats as these are generally  
 475 water saturated.

476 In addition to 6-methyl brGDGTs, the fractional abundances of brGDGTs  
 477 containing cyclopentane moieties (brGDGT-Ib and -IIb) are also significantly  
 478 correlated to pH (R = 0.73 and 0.56, p<0.01, respectively) (Fig. 7a and 7c). The other  
 479 brGDGTs are not significantly correlated to pH. These observations are consistent  
 480 with those from soils, where both 5- and 6-methyl brGDGTs containing cyclopentane  
 481 moieties are more abundant at higher pH (Weijers et al., 2007; Peterse et al., 2012; De  
 482 Jonge et al., 2014). Consequently, and similar to soils (De Jonge et al., 2014; Xiao et  
 483 al., 2015), CBT' (eq. 3) in peat can be modeled as a function of pH (Fig. 8):

$$eq. (10) \text{ pH} = 2.69 \times \text{CBT}' + 9.19 \quad (n = 50, R^2 = 0.44, \text{RMSE} = 1.0)$$

484 The slope of this calibration is different (higher) from that found in soils (see  
 485 supplementary information), but the coefficient of determination is lower, and the  
 486 RMSE is higher. A stronger correlation is obtained by using only compounds that are  
 487 significantly correlated to pH in the numerator, CBT<sub>peat</sub>:

$$eq. (11) \text{ CBT}_{peat} = \log \left( \frac{Ib + IIa' + IIb + IIb' + IIIa'}{Ia + IIa + IIIa} \right)$$

$$eq. (12) \text{ pH} = 2.49 \times \text{CBT}_{peat} + 8.07 \quad (n = 51, R^2 = 0.58, \text{RMSE} = 0.8)$$

488 Although the coefficient of determination increases and RMSE decreases using  
 489 CBT<sub>peat</sub>, the calibration uncertainties are still larger than those reported for soils (see  
 490 supplementary information).

491 It is noteworthy that in peats the correlation between brGDGT distributions  
 492 and pH is much weaker than that with MAAT (see below). This contrasts with  
 493 mineral soils, for which the correlation of CBT' with pH (R<sup>2</sup> = 0.85), is stronger than  
 494 that of MAT<sub>mr</sub> with MAAT (R<sup>2</sup> = 0.68) (De Jonge et al., 2014). The weaker  
 495 correlation can partly be explained by the smaller sample set used for the peat  
 496 calibration (n = 51) versus soil calibration (n = 221). However, taking 51 random  
 497 mineral soils from the latter still yields a stronger correlation between CBT' and pH  
 498 than we obtain for the peat data set. In addition, the coefficient of determination of a  
 499 calibration based only on peats with pH ≥ 5 is ~0.5 for CBT<sub>peat</sub>, similar to that of the  
 500 complete data set. We argue that the difference could be related to the observation  
 501 that in mineral soils water content also influences the brGDGT distribution, especially

502 that of 6-methyl brGDGTs (e.g., Menges et al., 2014). Recently Dang et al. (2016)  
503 showed that CBT<sub>(5me)</sub> is higher in dry soils compared to wet soils. Because alkaline  
504 soils are often also dry whereas acidic soils are often wet, this effect could enhance  
505 the correlation between CBT' and pH in soils. As peats are typically water saturated,  
506 the additional effect of soil water content is lacking, which may explain the weaker  
507 correlation between CBT' and pH in peats compared to mineral soils.

508

#### 509 4.2.2 Influence of MAAT on brGDGTs in peats

510 In mineral soils the distribution of brGDGTs is influenced by MAAT, with the degree  
511 of methylation decreasing as temperature increases (Weijers et al., 2007; De Jonge et  
512 al., 2014). A temperature effect on the brGDGT distribution was recently also found  
513 in one peatland (Huguet et al., 2013). Although the producers of brGDGTs are  
514 currently unknown, such a response is consistent with homeoviscous adaptation  
515 (Weijers et al., 2007). Here we investigate whether temperature has a significant  
516 correlation with brGDGTs in peats on a global scale.

517 When plotted against MAAT, only 5-methyl brGDGTs lacking cyclopentane  
518 moieties (brGDGT-Ia, -IIa, and -IIIa) have significant correlations with MAAT (Fig.  
519 9). brGDGT-Ia is positively correlated with MAAT ( $R = 0.72$ ,  $p < 0.01$ ), whereas  
520 brGDGT-IIa ( $R = 0.82$ ,  $p < 0.01$ ), and -IIIa ( $R = 0.63$ ,  $p < 0.01$ ) are negatively correlated  
521 with MAAT. These correlations are significantly higher than those found in the global  
522 soil data set (De Jonge et al., 2014). The degree of methylation of 5-methyl brGDGTs  
523 is captured in the MBT<sub>5me</sub>' index (eq. 2). As such we use the MBT<sub>5me</sub>' index to  
524 construct a peat-specific temperature proxy (Fig. 10):

$$\text{eq. (13) } MAAT_{peat} (\text{°C}) = 52.18 \times MBT'_{5me} - 23.05 \quad (n = 96, R^2 = 0.76, \text{RMSE} \\ = 4.7 \text{ °C})$$

525 Crucially, no correlation is observed between MBT<sub>5me</sub>' and pH ( $R^2 = 0$  and  $p > 0.8$ )  
526 and we observe no trend in the residuals. The coefficient of determination ( $R^2$ ) of  
527 MAAT<sub>peat</sub> is higher compared to a Deming regression of the expanded soil dataset ( $R^2$   
528 = 0.60, see supplementary information) as well as that of the linear MBT<sub>5me</sub>'  
529 calibration ( $R^2 = 0.66$ ) suggested by De Jonge et al. (2014). Crucially, because the  
530 slope of the MAAT<sub>peat</sub> calibration is steeper, it could have greater utility for the  
531 reconstruction of tropical temperatures (MAAT<sub>peat</sub> reaches saturation at 29.1 °C),  
532 although these maximum temperatures are higher than the maximum MAAT in the

533 modern calibration data set which is 26.7 °C. In contrast, the Deming MBT<sub>5me</sub>' soil  
534 calibration reaches saturation (i.e. MBT<sub>5me</sub>' = 1) at a temperature of 24.8 °C (see  
535 supplementary information), while the linear MBT<sub>5me</sub>' calibration suggested by De  
536 Jonge et al. (2014) has a maximum of 22.9 °C.

537

#### 538 *4.3 Implications for paleoclimate reconstructions and future work*

539 Compared to the natural archives previously used to reconstruct past terrestrial  
540 temperature change (e.g., riverine, lacustrine, and marine sediments), peats have a  
541 major advantage. For example, the brGDGTs in peat are mainly derived from *in situ*  
542 production. Mixing of brGDGT source areas, which complicates the application of  
543 GDGTs in sediments that represent a large catchment area (e.g., Zell et al., 2014; De  
544 Jonge et al., 2015; Sinninghe Damsté, 2016), is unlikely to be a problem. In addition,  
545 peats are overall characterized by anoxic conditions and the preservation potential of  
546 organic compounds such as brGDGTs is high. Finally, as peats are water saturated,  
547 especially the catotelm where the majority of brGDGT production occurs, the  
548 additional influence of changes in moisture content (Menges et al., 2014; Dang et al.,  
549 2016) is also negligible. Nevertheless, there are limitations to this proxy that need to  
550 be considered when evaluating suitable palaeoclimate applications, and we explore  
551 those below.

552

##### 553 *4.3.1 Late Holocene climate*

554 Here we provide peat-specific temperature and pH proxies that could be used to  
555 reconstruct terrestrial climate over a broad range of time scales, including the late  
556 Holocene. However, the estimated variation in terrestrial temperature of most places  
557 on earth during the last millennium is typically less than 1°C (Mann et al., 2009;  
558 Pages 2k Consortium, 2013), although there could be local exceptions. Such  
559 temperature change is much smaller than the calibration error (RMSE of ~ 4.7 °C).  
560 Although based on different lipids produced by different organisms, GDGT proxies  
561 can potentially record temperature changes smaller than the calibration errors when  
562 utilized within a highly constrained site-specific study (Tierney et al., 2010), although  
563 this interpretation was recently contested (Kraemer et al., 2015).

564       Regardless of calibration issues, application of the MAAT<sub>peat</sub> calibration to  
565 late Holocene palaeoclimate remains problematic. A potential seasonal bias in the top  
566 of some high-latitude peats, as well as a potential difference between oxic and anoxic

567 production, appear to prevent application of this proxy to shallow peat sediments.  
568 Indeed, our downcore profiles spanning the top 1 meter of peat exhibit changes in  
569 brGDGT distributions equivalent to temperature variations of up to several degrees  
570 Celsius, larger than the expected climate variations. Moreover, as discussed above,  
571 GDGTs appear to be predominantly generated at depth, and although this evidently  
572 ensures they record MAAT it does mean that their reconstructed temperature signals  
573 start in deeper peat horizons, i.e. stratigraphically preceding the climate changes that  
574 caused them.

575 Future work should determine whether these peat-specific proxies can be used  
576 to reconstruct small amplitude and/or short-lived temperature variation. However we  
577 currently urge caution in applying the peat-specific proxies to shallow peat cores to  
578 reconstruct late Holocene climate (e.g., Little Ice Age or Medieval Warm anomaly).  
579

#### 580 *4.3.2 Application to the last glacial*

581 We envision these proxies are well-suited to reconstruct large amplitude and more  
582 long-term temperature excursions such as those associated with the last glacial  
583 termination and early Holocene. Such transitions are recorded in some particularly  
584 long peat cores at several places around the world (e.g., McGlone et al., 2010;  
585 Vanneste et al., 2015; Zheng et al., 2015; Baker et al., 2016). To test whether the  
586 novel peat-specific temperature calibration can be used to reconstruct  
587 glacial/interglacial temperature variability, we applied this proxy to samples from the  
588 Hani peat sequence (Fig. 2). Hani peat is located in northeastern China and in places  
589 is up to 10 meters thick, spanning ~16,000 cal yrs (Zhou et al., 2010). We analyzed  
590 two samples from ~840 cm depth (corresponding to the late glacial at around 15.3  
591 kyr), and compared  $MAAT_{peat}$  with that of two samples from around 100 cm depth  
592 (corresponding to the late Holocene with an age of 700-1000 yrs). Using  $MAAT_{peat}$   
593 we obtained an average temperature of around -0.8 °C for the late glacial (15.3 kyr).  
594 For the late Holocene (0.7-1 kyr) we obtained an average temperature of around 4.6  
595 °C (Table 1).

596 Taking the calibration error of ~4.7 °C into account the reconstructed late  
597 Holocene temperatures (4.6 °C) are close to the observed modern-day MAAT of  
598 around 4 °C at this locality (Zhou et al., 2010). In contrast, applying soil calibrations  
599 to reconstruct MAAT at this site results in significantly higher values (up to 11 °C;  
600 Table 1).  $MAAT_{peat}$  (as well as the soil  $MBT_{5me}$  calibration) indicates that

601 temperatures increased from the late glacial to the late Holocene by around 5 °C. In  
602 contrast the MAT<sub>mr</sub> mineral soil calibration indicates a smaller increase of around 3  
603 °C. A ~ 5 °C increase is similar to that observed in east Asian loess-paleosol  
604 sequences (Peterse et al., 2014), although that is based on the MBT(′)/CBT method.  
605 In addition a 5 °C deglacial temperature increase is similar to those of several sea  
606 surface temperature records available from similar latitudes in the Sea of Japan (Lee,  
607 2007). The next step should be multiproxy temperature reconstructions in a variety of  
608 locations to test the new calibration and to determine whether absolute temperatures  
609 obtained using MAAT<sub>peat</sub> are reliable. Nonetheless, this initial analysis indicates that  
610 MAAT<sub>peat</sub> yields temperature estimates that are consistent with both modern day  
611 observations and other proxy estimates for the last glacial.

612

#### 613 *4.3.3 Deep time application*

614 We see considerable scope for future work with this proxy to reconstruct terrestrial  
615 temperature during past greenhouse periods and across hyperthermals (e.g.  
616 Paleocene/Eocene Thermal Maximum; PETM). These events are recorded in lignite  
617 deposits. For example the PETM is documented in lignites from the UK (Collinson et  
618 al., 2003; Pancost et al., 2007). Importantly, lignites are the lowest (maturity) rank of  
619 coal and have not experienced significant burial and associated temperature and  
620 pressure that leads to the loss of GDGTs (Schouten et al., 2004, 2013). Due to their  
621 low thermal maturity, lignites are thought to retain their original brGDGT distribution  
622 over geological timescales. For example, brGDGTs have been reported in an  
623 immature late Paleocene lignite from the USA (Weijers et al., 2011), early Eocene  
624 lignites from Germany (Inglis et al., 2017), as well as Miocene lignite from Germany  
625 (Stock et al., 2016). Although analyzed using the classical analytical method that did  
626 not separate 5 and 6-methyl brGDGTs, the brGDGT distribution in a late Paleocene  
627 lignite from North America is dominated by brGDGT-Ia (Weijers et al., 2011),  
628 similar to that seen in modern peats from the tropics and suggesting high terrestrial  
629 temperatures. This is consistent with our overall understanding of terrestrial climate  
630 during the greenhouse world of the late Paleocene and early Eocene (Huber and  
631 Caballero, 2011).

632 As the brGDGT distribution in peat deposits is dominated by production in the  
633 anoxic catotelm below the water table where the seasonal temperature cycle is muted  
634 (see section 4.1) brGDGT-based temperatures obtained from lignite deposits can be

635 considered to reflect MAAT. We envision that future studies applying our new peat-  
636 specific calibrations to immature lignites will provide valuable new insights into  
637 terrestrial climate during the geological past. In addition, the GDGT concentrations in  
638 peats are generally much higher than those found in soils. We therefore propose that  
639 for studies of brGDGT distributions in (marine) sediments with a peat-dominated  
640 catchment area (e.g. Siberia (Frey and Smith, 2005)) or that contain independent  
641 evidence for the input of peat-derived material (e.g. high concentration of C<sub>31</sub> αβ-  
642 hopanes or palynologic evidence for the input of typical peatland vegetation), the  
643 majority of GDGTs is likely derived from peatlands. In such settings it is more  
644 appropriate to use a peat-specific calibration rather than a mineral soil calibration.

645

## 646 **5. Conclusions**

647 Using 470 samples from 96 peatlands from around the world we explored the  
648 environmental controls on the bacterial brGDGT distribution in peats. We  
649 demonstrate that brGDGT distributions are correlated with peat pH and especially  
650 mean annual air temperature (MAAT). We develop for the first time peat-specific  
651 brGDGT-derived pH and temperature calibrations. In addition to their application in  
652 ancient peat-forming environments, we also suggest that these calibrations could be  
653 preferable to the available mineral soil calibration in marginal marine settings when it  
654 is clear that brGDGTs are predominantly derived from peats. We suggest caution in  
655 applying this proxy to late Holocene peat (e.g., covering the Medieval Climatic  
656 Anomaly and/or Little Ice Age) as both the calibration error and downcore variation  
657 appears to be larger than expected climate signals during this period. Taken together  
658 our results demonstrate that there is clear potential to use GDGTs in peatlands and  
659 lignites to reconstruct past terrestrial climate, opening up a new set of sedimentary  
660 archives that will help to improve understanding of the climate system during the  
661 geological past.

662

## 663 **Acknowledgements**

664 This research was funded through the advanced ERC grant “the greenhouse earth  
665 system” (T-GRES, project reference 340923), awarded to RDP. All authors are part of  
666 the “T-GRES Peat Database collaborators” collective. RDP also acknowledges the  
667 Royal Society Wolfson Research Merit Award. We thank D. Atkinson for help with  
668 the sample preparation. We acknowledge support from Labex VOLTAIRE (ANR-10-

669 LABX-100-01). Peat from Patagonia and Tierra del Fuego were collected thanks to a  
670 Young Researcher Grant of the Agence National de la Recherche (ANR) to FDV,  
671 project ANR-2011-JS56-006-01 “PARAD” and with the help of Ramiro Lopez,  
672 Andrea Coronato and Veronica Pancotto (CADIC-CONICET, Ushuaia). Peat from  
673 Brazil was collected with the context of CNPq project 482815/2011-6. Samples from  
674 France (Frasne and La Gnette) were collected thanks to the French Observatory of  
675 Peatlands. The Canadian peat was collected in the context of the NSERC-Discovery  
676 grant of L. Rochefort. Peats from China were obtained under a National Natural  
677 Science Foundation of China grant (No. 41372033), awarded to Y. Zheng. We thank  
678 the editor, 3 anonymous reviewers, and Jess Tierney for valuable comments.

679

#### 680 **References:**

- 681 Adcock, R.J., 1878. A Problem in Least Squares. *Analyst* **5** (2), 53-54.  
682  
683 Baird, A.J., Milner, A.M., Blundell, A., Swindles, G.T., Morris, P.J., 2016.  
684 Microform-scale variations in peatland permeability and their ecohydrological  
685 implications. *J. Ecol.* **104** (2), 531-544.  
686  
687 Baker, A., Routh, J., Roychoudhury, A.N., 2016. Biomarker records of  
688 palaeoenvironmental variations in subtropical Southern Africa since the late  
689 Pleistocene: Evidences from a coastal peatland. *Palaeogeogr. Palaeoclimatol.*  
690 *Palaeoecol.* **451**, 1-12.  
691  
692 Ballantyne, A.P., Greenwood, D.R., Sinninghe Damsté, J.S., Csank, A.Z., Eberle, J.J.,  
693 Rybczynski, N., 2010. Significantly warmer Arctic surface temperatures during the  
694 Pliocene indicated by multiple independent proxies. *Geology* **38** (7), 603-606.  
695  
696 Barber, K.E., 1993. Peatlands as scientific archives of past biodiversity. *Biodivers.*  
697 *Conserv.* **2** (5), 474-489.  
698  
699 Burrows, M.A., Fenner, J., Haberle, S.G., 2014. Humification in northeast Australia:  
700 Dating millennial and centennial scale climate variability in the late Holocene.  
701 *Holocene* **24** (12), 1707-1718.  
702  
703 Chambers, F.M., Charman, D.J., 2004. Holocene environmental change: contributions  
704 from the peatland archive. *Holocene* **14** (1), 1-6.  
705  
706 Chambers, F.M., Booth, R.K., De Vleeschouwer, F., Lamentowicz, M., Le Roux, G.,  
707 Mauquoy, D., Nichols, J.E., et al., 2012. Development and refinement of proxy-  
708 climate indicators from peats. *Quatern. Int.* **268**, 21-33.  
709  
710 Chambers, F.M., Brain, S.A., Mauquoy, D., McCarroll, J., Daley, T., 2014. The  
711 ‘Little Ice Age’ in the Southern Hemisphere in the context of the last 3000 years:  
712 Peat-based proxy-climate data from Tierra del Fuego. *Holocene* **24** (12), 1649-1656.

713  
714 Chaves Torres, L., Pancost, R.D., 2016. Insoluble prokaryotic membrane lipids in a  
715 *Sphagnum* peat: Implications for organic matter preservation. *Org. Geochem.* **93**, 77-  
716 91.  
717  
718 Collinson, M.E., Hooker, J.J., Gröcke, D.R., 2003. Cobham Lignite Bed and  
719 penecontemporaneous macrofloras of southern England: A record of vegetation and  
720 fire across the Paleocene-Eocene Thermal Maximum, in: Wing, S.L., Gingerich, P.D.,  
721 Schmitz, B., Thomas, B. (Eds.), Causes and Consequences of Globally Warm  
722 Climates in the Early Paleogene. Geological Society of America, Boulder, Colorado,  
723 pp. 333-349.  
724  
725 Cristea, G., Cuna, S.M., Fărcaș, S., Tanțău, I., Dordai, E., Măgdaș, D.A., 2014.  
726 Carbon isotope composition as an indicator of climatic changes during the middle and  
727 late Holocene in a peat bog from the Maramureș Mountains (Romania). *Holocene* **24**,  
728 15-23.  
729  
730 Dang, X., Yang, H., Naafs, B.D.A., Pancost, R.D., Evershed, R.P., Xie, S., 2016.  
731 Direct evidence of moisture control on the methylation of branched glycerol dialkyl  
732 glycerol tetraethers in semi-arid and arid soils. *Geochim. Cosmochim. Acta* **189**, 24-  
733 36.  
734  
735 De Jonge, C., Hopmans, E.C., Stadnitskaia, A., Rijpstra, W.I.C., Hofland, R.,  
736 Tegelaar, E., Sinninghe Damsté, J.S., 2013. Identification of novel penta- and  
737 hexamethylated branched glycerol dialkyl glycerol tetraethers in peat using HPLC-  
738 MS<sup>2</sup>, GC-MS and GC-SMB-MS. *Org. Geochem.* **54**, 78-82.  
739  
740 De Jonge, C., Hopmans, E.C., Zell, C.I., Kim, J.-H., Schouten, S., Sinninghe Damsté,  
741 J.S., 2014. Occurrence and abundance of 6-methyl branched glycerol dialkyl glycerol  
742 tetraethers in soils: implications for palaeoclimate reconstruction. *Geochim.*  
743 *Cosmochim. Acta* **141**, 97-112.  
744  
745 De Jonge, C., Stadnitskaia, A., Hopmans, E.C., Cherkashov, G., Fedotov, A.,  
746 Streletskaya, I.D., Vasiliev, A.A., et al., 2015. Drastic changes in the distribution of  
747 branched tetraether lipids in suspended matter and sediments from the Yenisei River  
748 and Kara Sea (Siberia): Implications for the use of brGDGT-based proxies in coastal  
749 marine sediments. *Geochim. Cosmochim. Acta* **165**, 200-225.  
750  
751 Ding, S., Xu, Y., Wang, Y., He, Y., Hou, J., Chen, L., He, J.S., 2015. Distribution of  
752 branched glycerol dialkyl glycerol tetraethers in surface soils of the Qinghai-Tibetan  
753 Plateau: implications of brGDGTs-based proxies in cold and dry regions.  
754 *Biogeosciences* **12** (11), 3141-3151.  
755  
756 Frey, K.E., Smith, L.C., 2005. Amplified carbon release from vast West Siberian  
757 peatlands by 2100. *Geophys. Res. Lett.* **32** (9), L09401.  
758  
759 Gallego-Sala, A.V., Prentice, C.I., 2013. Blanket peat biome endangered by climate  
760 change. *Nat. Clim. Chang.* **3** (2), 152-155.  
761

762 Gorham, E., Janssens, J.A., Glaser, P.H., 2003. Rates of peat accumulation during the  
763 postglacial period in 32 sites from Alaska to Newfoundland, with special emphasis on  
764 northern Minnesota. *Can. J. Bot.* **81** (5), 429-438.  
765

766 Hansson, S.V., Bindler, R., De Vleeschouwer, F., 2015. Using Peat Records as  
767 Natural Archives of Past Atmospheric Metal Deposition, in: Blais, J.M., Rosen, M.R.,  
768 Smol, J.P. (Eds.), *Environmental Contaminants*. Springer Netherlands, pp. 323-354.  
769

770 Hillel, D., 1982. *Introduction to Soil Physics*. Academic Press, New York.  
771

772 Hopmans, E.C., Weijers, J.W.H., Schefuß, E., Herfort, L., Sinninghe Damsté, J.S.,  
773 Schouten, S., 2004. A novel proxy for terrestrial organic matter in sediments based on  
774 branched and isoprenoid tetraether lipids. *Earth Plant. Sc. Lett.* **224** (1-2), 107-116.  
775

776 Hopmans, E.C., Schouten, S., Sinninghe Damsté, J.S., 2016. The effect of improved  
777 chromatography on GDGT-based palaeoproxies. *Org. Geochem.* **93**, 1-6.  
778

779 Huber, M., Caballero, R., 2011. The early Eocene equable climate problem revisited.  
780 *Clim. Past* **7** (2), 603-633.  
781

782 Huguet, A., Fosse, C., Laggoun-Défarge, F., Toussaint, M.-L., Derenne, S., 2010.  
783 Occurrence and distribution of glycerol dialkyl glycerol tetraethers in a French peat  
784 bog. *Org. Geochem.* **41** (6), 559-572.  
785

786 Huguet, A., Fosse, C., Laggoun-Défarge, F., Delarue, F., Derenne, S., 2013. Effects of  
787 a short-term experimental microclimate warming on the abundance and distribution of  
788 branched GDGTs in a French peatland. *Geochim. Cosmochim. Acta* **105**, 294-315.  
789

790 Huguet, A., Francez, A.-J., Jusselme, M.D., Fosse, C., Derenne, S., 2014. A climatic  
791 chamber experiment to test the short term effect of increasing temperature on  
792 branched GDGT distribution in *Sphagnum* peat. *Org. Geochem.* **73**, 109-112.  
793

794 Inglis, G.N., Collinson, M.E., Riegel, W., Wilde, V., Farnsworth, A., Lunt, D.J.,  
795 Valdes, P., et al., 2017. Mid-latitude continental temperatures through the early  
796 Eocene in western Europe. *Earth Plant. Sc. Lett.* **460**, 86-96.  
797

798 Kaplan, J.O., Bigelow, N.H., Prentice, I.C., Harrison, S.P., Bartlein, P.J., Christensen,  
799 T.R., Cramer, W., et al., 2003. Climate change and Arctic ecosystems: 2. Modeling,  
800 paleodata-model comparisons, and future projections. *J. Geophys. Res.-Atmos.* **108**  
801 (D19).  
802

803 Kraemer, B.M., Hook, S., Huttula, T., Kotilainen, P., O'Reilly, C.M., Peltonen, A.,  
804 Plisnier, P.-D., et al., 2015. Century-Long Warming Trends in the Upper Water  
805 Column of Lake Tanganyika. *PLOS ONE* **10** (7), e0132490.  
806

807 Lafleur, P.M., Moore, T.R., Roulet, N.T., Frohling, S., 2005. Ecosystem Respiration  
808 in a Cool Temperate Bog Depends on Peat Temperature But Not Water Table.  
809 *Ecosystems* **8** (6), 619-629.  
810

811 Laiho, R., 2006. Decomposition in peatlands: Reconciling seemingly contrasting  
812 results on the impacts of lowered water levels. *Soil Biol. Biochem.* **38** (8), 2011-2024.  
813

814 Lee, K.E., 2007. Surface water changes recorded in Late Quaternary marine  
815 sediments of the Ulleung Basin, East Sea (Japan Sea). *Palaeogeogr. Palaeoclimatol.*  
816 *Palaeoecol.* **247** (1–2), 18-31.  
817

818 Lei, Y., Yang, H., Dang, X., Zhao, S., Xie, S., 2016. Absence of a significant bias  
819 towards summer temperature in branched tetraether-based paleothermometer at two  
820 soil sites with contrasting temperature seasonality. *Org. Geochem.* **94**, 83-94.  
821

822 Li, J., Pancost, R.D., Naafs, B.D.A., Yang, H., Zhao, C., Xie, S., 2016. Distribution of  
823 glycerol dialkyl glycerol tetraether (GDGT) lipids in a hypersaline lake system. **99**,  
824 113-124.  
825

826 Liu, X.-L., Leider, A., Gillespie, A., Gröger, J., Versteegh, G.J.M., Hinrichs, K.-U.,  
827 2010. Identification of polar lipid precursors of the ubiquitous branched GDGT  
828 orphan lipids in a peat bog in Northern Germany. *Org. Geochem.* **41** (7), 653-660.  
829

830 Loomis, S.E., Russell, J.M., Sinninghe Damsté, J.S., 2011. Distributions of branched  
831 GDGTs in soils and lake sediments from western Uganda: Implications for a  
832 lacustrine paleothermometer. *Org. Geochem.* **42** (7), 739-751.  
833

834 Loomis, S.E., Russell, J.M., Eggermont, H., Verschuren, D., Sinninghe Damsté, J.S.,  
835 2014. Effects of temperature, pH and nutrient concentration on branched GDGT  
836 distributions in East African lakes: Implications for paleoenvironmental  
837 reconstruction. *Org. Geochem.* **66**, 25-37.  
838

839 Mann, M.E., Zhang, Z., Rutherford, S., Bradley, R.S., Hughes, M.K., Shindell, D.,  
840 Ammann, C., et al., 2009. Global Signatures and Dynamical Origins of the Little Ice  
841 Age and Medieval Climate Anomaly. *Science* **326** (5957), 1256-1260.  
842

843 Manuilova, E., Schuetzenmeister, A., Model, F., 2014. Method Comparison  
844 Regression. CRAN, <https://cran.r-project.org/web/packages/mcr/index.html>.  
845

846 Mauquoy, D., Yeloff, D., Van Geel, B., Charman, D.J., Blundell, A., 2008. Two  
847 decadal resolved records from north-west European peat bogs show rapid climate  
848 changes associated with solar variability during the mid–late Holocene. *J. Quat. Sci.*  
849 **23** (8), 745-763.  
850

851 McGlone, M.S., Turney, C.S.M., Wilmshurst, J.M., Renwick, J., Pahnke, K., 2010.  
852 Divergent trends in land and ocean temperature in the Southern Ocean over the past  
853 18,000 years. *Nat. Geosci.* **3** (9), 622-626.  
854

855 McKenzie, J.M., Siegel, D.I., Rosenberry, D.O., Glaser, P.H., Voss, C.I., 2007. Heat  
856 transport in the Red Lake Bog, Glacial Lake Agassiz Peatlands. *Hydrol. Process.* **21**  
857 (3), 369-378.  
858

859 Menges, J., Huguet, C., Alcañiz, J.M., Fietz, S., Sachse, D., Rosell-Melé, A., 2014.  
860 Influence of water availability in the distributions of branched glycerol dialkyl

861 glycerol tetraether in soils of the Iberian Peninsula. *Biogeosciences* **11** (10), 2571-  
862 2581.

863

864 New, M., Hulme, M., Jones, P., 1999. Representing Twentieth-Century Space–Time  
865 Climate Variability. Part I: Development of a 1961–90 Mean Monthly Terrestrial  
866 Climatology. *J. Climate* **12** (3), 829-856.

867

868 Nichols, J.E., Booth, R.K., Jackson, S.T., Pendall, E.G., Huang, Y., 2006.  
869 Paleohydrologic reconstruction based on *n*-alkane distributions in ombrotrophic peat.  
870 *Org. Geochem.* **37** (11), 1505-1513.

871

872 Pages 2k Consortium, 2013. Continental-scale temperature variability during the past  
873 two millennia. *Nat. Geosci.* **6** (5), 339-346.

874

875 Pancost, R.D., Baas, M., van Geel, B., Sinninghe Damsté, J.S., 2003. Response of an  
876 ombrotrophic bog to a regional climate event revealed by macrofossil, molecular and  
877 carbon isotopic data. *Holocene* **13** (6), 921-932.

878

879 Pancost, R.D., Steart, D.S., Handley, L., Collinson, M.E., Hooker, J.J., Scott, A.C.,  
880 Grassineau, N.V., et al., 2007. Increased terrestrial methane cycling at the Palaeocene-  
881 Eocene thermal maximum. *Nature* **449** (7160), 332-335.

882

883 Pancost, R.D., McClymont, E.L., Bingham, E.M., Roberts, Z., Charman, D.J.,  
884 Hornibrook, E.R.C., Blundell, A., et al., 2011. Archaeol as a methanogen biomarker  
885 in ombrotrophic bogs. *Org. Geochem.* **42** (10), 1279-1287.

886

887 Peterse, F., Hopmans, E.C., Schouten, S., Mets, A., Rijpstra, W.I.C., Sinninghe  
888 Damsté, J.S., 2011. Identification and distribution of intact polar branched tetraether  
889 lipids in peat and soil. *Org. Geochem.* **42** (9), 1007-1015.

890

891 Peterse, F., van der Meer, J., Schouten, S., Weijers, J.W.H., Fierer, N., Jackson, R.B.,  
892 Kim, J.-H., et al., 2012. Revised calibration of the MBT–CBT paleotemperature proxy  
893 based on branched tetraether membrane lipids in surface soils. *Geochim. Cosmochim.*  
894 *Acta* **96**, 215-229.

895

896 Peterse, F., Martínez-García, A., Zhou, B., Beets, C.J., Prins, M.A., Zheng, H.,  
897 Eglinton, T.I., 2014. Molecular records of continental air temperature and monsoon  
898 precipitation variability in East Asia spanning the past 130,000 years. *Quaternary Sci.*  
899 *Rev.* **83**, 76-82.

900

901 Roland, T.P., Daley, T.J., Caseldine, C.J., Charman, D.J., Turney, C.S.M., Amesbury,  
902 M.J., Thompson, G.J., et al., 2015. The 5.2 ka climate event: Evidence from stable  
903 isotope and multi-proxy palaeoecological peatland records in Ireland. *Quat. Sci. Rev.*  
904 **124**, 209-223.

905

906 RStudio Team, 2015. RStudio: Integrated Development for R. RStudio, Inc., Boston,  
907 MA (USA).

908

909 Schellekens, J., Bindler, R., Martínez-Cortizas, A., McClymont, E.L., Abbott, G.D.,  
910 Biester, H., Pontevedra-Pombal, X., et al., 2015. Preferential degradation of

911 polyphenols from *Sphagnum* – 4-Isopropenylphenol as a proxy for past hydrological  
912 conditions in *Sphagnum*-dominated peat. *Geochim. Cosmochim. Acta* **150**, 74-89.  
913  
914 Schoon, P.L., de Kluijver, A., Middelburg, J.J., Downing, J.A., Sinninghe Damsté,  
915 J.S., Schouten, S., 2013. Influence of lake water pH and alkalinity on the distribution  
916 of core and intact polar branched glycerol dialkyl glycerol tetraethers (GDGTs) in  
917 lakes. *Org. Geochem.* **60**, 72-82.  
918  
919 Schouten, S., Hopmans, E.C., Pancost, R.D., Sinninghe Damsté, J.S., 2000.  
920 Widespread occurrence of structurally diverse tetraether membrane lipids: Evidence  
921 for the ubiquitous presence of low-temperature relatives of hyperthermophiles. *Proc.*  
922 *Natl. Acad. Sci.* **97** (26), 14421-14426.  
923  
924 Schouten, S., Hopmans, E.C., Sinninghe Damsté, J.S., 2004. The effect of maturity  
925 and depositional redox conditions on archaeal tetraether lipid palaeothermometry.  
926 *Org. Geochem.* **35** (5), 567-571.  
927  
928 Schouten, S., Hopmans, E.C., Sinninghe Damsté, J.S., 2013. The organic  
929 geochemistry of glycerol dialkyl glycerol tetraether lipids: A review. *Org. Geochem.*  
930 **54**, 19-61.  
931  
932 Sinninghe Damsté, J.S., Hopmans, E.C., Pancost, R.D., Schouten, S., Geenevasen,  
933 J.A.J., 2000. Newly discovered non-isoprenoid glycerol dialkyl glycerol tetraether  
934 lipids in sediments. *Chem. Commun.*(17), 1683-1684.  
935  
936 Sinninghe Damsté, J.S., Schouten, S., Hopmans, E.C., van Duin, A.C.T., Geenevasen,  
937 J.A.J., 2002. Crenarchaeol: the characteristic core glycerol dibiphytanyl glycerol  
938 tetraether membrane lipid of cosmopolitan pelagic crenarchaeota. *J. Lipid. Res.* **43**  
939 (10), 1641-1651.  
940  
941 Sinninghe Damsté, J.S., Rijpstra, W.I.C., Hopmans, E.C., Weijers, J.W.H., Foesel,  
942 B.U., Overmann, J., Dedysh, S.N., 2011. 13,16-Dimethyl Octacosanedioic Acid (*iso*-  
943 Diabolic Acid), a Common Membrane-Spanning Lipid of *Acidobacteria* Subdivisions  
944 1 and 3. *Appl. Environ. Microb.* **77** (12), 4147-4154.  
945  
946 Sinninghe Damsté, J.S., Rijpstra, W.I.C., Hopmans, E.C., Foesel, B.U., Wüst, P.K.,  
947 Overmann, J., Tank, M., et al., 2014. Ether- and Ester-Bound *iso*-Diabolic Acid and  
948 Other Lipids in Members of *Acidobacteria* Subdivision 4. *Appl. Environ. Microb.* **80**  
949 (17), 5207-5218.  
950  
951 Sinninghe Damsté, J.S., 2016. Spatial heterogeneity of sources of branched tetraethers  
952 in shelf systems: The geochemistry of tetraethers in the Berau River delta  
953 (Kalimantan, Indonesia). *Geochim. Cosmochim. Acta* **186**, 13-31.  
954  
955 Stanek, W., 1973. Comparisons of methods of pH determination for organic terrain  
956 surveys. *Can. J. Soil Sci.* **53** (2), 177-183.  
957  
958 Stock, A.T., Littke, R., Lücke, A., Zieger, L., Thielemann, T., 2016. Miocene  
959 depositional environment and climate in western Europe: The lignite deposits of the  
960 Lower Rhine Basin, Germany. *Int. J. Coal. Geol.* **157**, 2-18.

961  
962 Tierney, J.E., Mayes, M.T., Meyer, N., Johnson, C., Swarzenski, P.W., Cohen, A.S.,  
963 Russell, J.M., 2010. Late-twentieth-century warming in Lake Tanganyika  
964 unprecedented since AD 500. *Nat. Geosci.* **3** (6), 422-425.  
965  
966 Tierney, J.E., Schouten, S., Pitcher, A., Hopmans, E.C., Sinninghe Damsté, J.S.,  
967 2012. Core and intact polar glycerol dialkyl glycerol tetraethers (GDGTs) in Sand  
968 Pond, Warwick, Rhode Island (USA): Insights into the origin of lacustrine GDGTs.  
969 *Geochim. Cosmochim. Acta* **77**, 561-581.  
970  
971 Väiliranta, M., Blundell, A., Charman, D.J., Karofeld, E., Korhola, A., Sillasoo, Ü.,  
972 Tuittila, E.S., 2012. Reconstructing peatland water tables using transfer functions for  
973 plant macrofossils and testate amoebae: A methodological comparison. *Quat. Int.* **268**,  
974 34-43.  
975  
976 Vanneste, H., De Vleeschouwer, F., Martínez-Cortizas, A., von Scheffer, C.,  
977 Piotrowska, N., Coronato, A., Le Roux, G., 2015. Late-glacial elevated dust  
978 deposition linked to westerly wind shifts in southern South America. *Sci. Rep.* **5**,  
979 11670  
980  
981 Vitt, D.H., Bayley, S.E., Jin, T.-L., 1995. Seasonal variation in water chemistry over a  
982 bog-rich fen gradient in Continental Western Canada. *Can. J. Fish. Aquat. Sci.* **52** (3),  
983 587-606.  
984  
985 Weijers, J.W.H., Schouten, S., van der Linden, M., van Geel, B., Sinninghe Damsté,  
986 J.S., 2004. Water table related variations in the abundance of intact archaeal  
987 membrane lipids in a Swedish peat bog. *FEMS Microbiol. Lett.* **239** (1), 51-56.  
988  
989 Weijers, J.W.H., Schouten, S., Hopmans, E.C., Geenevasen, J.A.J., David, O.R.P.,  
990 Coleman, J.M., Pancost, R.D., et al., 2006a. Membrane lipids of mesophilic anaerobic  
991 bacteria thriving in peats have typical archaeal traits. *Environ. Microbiol.* **8** (4), 648-  
992 657.  
993  
994 Weijers, J.W.H., Schouten, S., Spaargaren, O.C., Sinninghe Damsté, J.S., 2006b.  
995 Occurrence and distribution of tetraether membrane lipids in soils: Implications for  
996 the use of the TEX<sub>86</sub> proxy and the BIT index. *Org. Geochem.* **37** (12), 1680-1693.  
997  
998 Weijers, J.W.H., Schouten, S., van den Donker, J.C., Hopmans, E.C., Sinninghe  
999 Damsté, J.S., 2007. Environmental controls on bacterial tetraether membrane lipid  
1000 distribution in soils. *Geochim. Cosmochim. Acta* **71** (3), 703-713.  
1001  
1002 Weijers, J.W.H., Panoto, E., van Bleijswijk, J., Schouten, S., Rijpstra, W.I.C., Balk,  
1003 M., Stams, A.J.M., et al., 2009. Constraints on the Biological Source(s) of the Orphan  
1004 Branched Tetraether Membrane Lipids. *Geomicrobiol. J.* **26** (6), 402-414.  
1005  
1006 Weijers, J.W.H., Steinmann, P., Hopmans, E.C., Schouten, S., Sinninghe Damsté,  
1007 J.S., 2011. Bacterial tetraether membrane lipids in peat and coal: Testing the MBT-  
1008 CBT temperature proxy for climate reconstruction. *Org. Geochem.* **42** (5), 477-486.  
1009

- 1010 Woillard, G.M., 1978. Grande Pile peat bog: A continuous pollen record for the last  
1011 140,000 years. *Quaternary Res.* **9** (1), 1-21.
- 1012
- 1013 Xiao, W., Xu, Y., Ding, S., Wang, Y., Zhang, X., Yang, H., Wang, G., et al., 2015.  
1014 Global calibration of a novel, branched GDGT-based soil pH proxy. *Org. Geochem.*  
1015 **89–90**, 56-60.
- 1016
- 1017 Xie, S., Pancost, R.D., Chen, L., Evershed, R.P., Yang, H., Zhang, K., Huang, J., et  
1018 al., 2012. Microbial lipid records of highly alkaline deposits and enhanced aridity  
1019 associated with significant uplift of the Tibetan Plateau in the Late Miocene. *Geology*  
1020 **40** (4), 291-294.
- 1021
- 1022 Yang, H., Lü, X., Ding, W., Lei, Y., Dang, X., Xie, S., 2015. The 6-methyl branched  
1023 tetraethers significantly affect the performance of the methylation index (MBT') in  
1024 soils from an altitudinal transect at Mount Shennongjia. *Org. Geochem.* **82**, 42-53.
- 1025
- 1026 Yvon-Durocher, G., Allen, A.P., Bastviken, D., Conrad, R., Gudas, C., St-Pierre, A.,  
1027 Thanh-Duc, N., et al., 2014. Methane fluxes show consistent temperature dependence  
1028 across microbial to ecosystem scales. *Nature* **507** (7493), 488-491.
- 1029
- 1030 Zell, C., Kim, J.H., Balsinha, M., Dorhout, D., Fernandes, C., Baas, M., Sinninghe  
1031 Damsté, J.S., 2014. Transport of branched tetraether lipids from the Tagus River basin  
1032 to the coastal ocean of the Portuguese margin: consequences for the interpretation of  
1033 the MBT'/CBT paleothermometer. *Biogeosciences* **11** (19), 5637-5655.
- 1034
- 1035 Zheng, Y., Li, Q., Wang, Z., Naafs, B.D.A., Yu, X., Pancost, R.D., 2015. Peatland  
1036 GDGT records of Holocene climatic and biogeochemical responses to the Asian  
1037 Monsoon. *Org. Geochem.* **87**, 86-95.
- 1038
- 1039 Zhou, W., Zheng, Y., Meyers, P.A., Jull, A.J.T., Xie, S., 2010. Postglacial climate-  
1040 change record in biomarker lipid compositions of the Hani peat sequence,  
1041 Northeastern China. *Earth Planet. Sc. Lett.* **294** (1–2), 37-46.
- 1042
- 1043 Zocatelli, R., Jacob, J., Gogo, S., Le Milbeau, C., Rousseau, J., Laggoun-Défarge, F.,  
1044 2014. Spatial variability of soil lipids reflects vegetation cover in a French peatland.  
1045 *Org. Geochem.* **76**, 173-183.

1046  
1047

#### 1048 **Figure captions**

1049 Fig. 1: Structures of brGDGTs (with numbering) as well as isoprenoidal GDGT  
1050 crenarchaeol (cren), following (De Jonge et al., 2014). Roman numbers indicate tetra-  
1051 (I), penta- (II), and hexamethylated (III) brGDGTs, whereas letters indicate the  
1052 absence (a), presence of one (b), or two (c) cyclopentane rings. Prime symbols  
1053 indicate 6-methyl brGDGTs in which the additional methyl groups of the penta- and  
1054 hexamethylated brGDGTs occur at the  $\alpha$  and/or  $\omega$ -6 position instead of  $\alpha$  and/or  $\omega$ -5  
1055 position of 5-methyl brGDGTs.

1056

1057 Fig. 2: Map with the location of all peats used in this study. The star indicates the  
1058 location of the Hani peat sequence in NE China.

1059

1060 Fig. 3: Fractional abundances of the three main brGDGTs in the top 15 cm of each  
1061 peat (assumed to be representative of the oxic acrotelm) versus the fractional  
1062 abundance of these brGDGTs between 15 and 100 cm in the peat (assumed to be  
1063 representative for the anoxic catotelm). For peats where multiple samples were  
1064 analyzed, error bars represent  $1\sigma$  from the average fractional abundance.

1065

1066 Fig. 4: Down core record of  $MBT_{5me}'$  in four peats: a high-latitude peat from Sweden  
1067 (blue squares), high-latitude peat from Patagonia (orange squares), temperate peat  
1068 from the UK (green triangles), and tropical peat from Indonesia (purple diamonds).  
1069 (For interpretation of the references to color in this figure legend, the reader is  
1070 referred to the web version of this article.)

1071

1072 Fig. 5: Standard deviation of  $MBT_{5me}'$  for each low-altitude ( $< 1000$  m) peat versus  
1073 latitude. The four peats used in figure 4 are highlighted.

1074

1075 Figure 6: Ratio of 6-methyl over 5-methyl brGDGTs ( $IR_{6me}$ ) versus pH for peat  
1076 samples (black squares) together with the  $IR_{6me}$  in the top 10 cm of mineral soils  
1077 (orange circles) (De Jonge et al., 2014; Ding et al., 2015; Xiao et al., 2015; Yang et  
1078 al., 2015; Lei et al., 2016). Vertical error bars on the peat data represent  $1\sigma$  and are  
1079 based on the analysis of multiple horizons from the same peat. Horizontal error bars  
1080 represent the spread in pH reported for each peat. (For interpretation of the references  
1081 to color in this figure legend, the reader is referred to the web version of this article.)

1082

1083 Figure 7: Fractional abundance of brGDGT versus pH for those compounds with a r-  
1084 value greater than 0.45 A) brGDGT-Ib, B) brGDGT-IIa', C) brGDGT-IIb, D)  
1085 brGDGT-IIb', and E) brGDGT-IIIa' ( $p < 0.01$  for all compounds). Samples with  
1086 fractional abundances  $< 0.001$  are not included. Vertical error bars represent  $1\sigma$  and  
1087 are based on the analysis of multiple horizons from the same peat. Horizontal error  
1088 bars represent the spread in pH reported for each peat.

1089

1090 Fig. 8: A) Average CBT' for each peat versus pH (black circles) and C) average  
1091 CBT<sub>peat</sub> for each peat versus pH (black circles). Solid blue lines in A and C represent  
1092 the Deming regression used to obtain the calibrations, while dashed black lines reflect  
1093 simple linear regressions. Horizontal error bars represent 1 $\sigma$  and are based on the  
1094 analysis of horizons samples from the same peat. Vertical error bars represent the  
1095 spread in pH reported for each peat. Also shown is the residual pH for all analyzed  
1096 peat samples (yellow circles), obtained by subtracting the estimated pH using the  
1097 CBT' (B) and CBT<sub>peat</sub> (D) deming calibrations from the observed pH. (For  
1098 interpretation of the references to color in this figure legend, the reader is referred to  
1099 the web version of this article.)

1100

1101 Fig. 9: Fractional abundance of the three main brGDGT versus MAAT A) brGDGT-  
1102 Ia, B) brGDGT-IIa, and C) brGDGT-IIIa ( $p < 0.01$  for all compounds). Samples with  
1103 fractional abundances  $< 0.001$  were not included. Vertical error bars represent 1 $\sigma$  and  
1104 are based on the analysis of multiple horizons from the same peat.

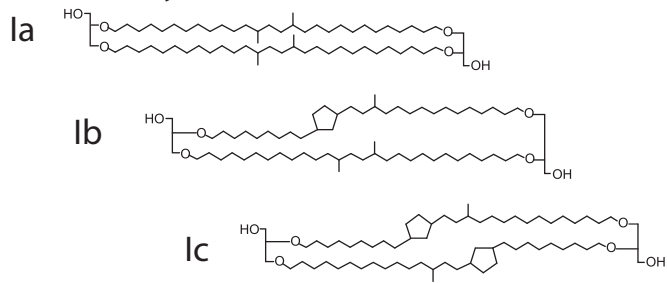
1105

1106 Fig. 10: Average MBT<sub>5me</sub>' for each peat versus MAAT (black circles). The solid blue  
1107 line represents the Deming regression, whereas dashed lines reflect the simple linear  
1108 regression. Horizontal error bars represent 1 $\sigma$  and are based on the analysis of  
1109 multiple horizons from the same peat. Also shown is the residual MAAT of all  
1110 analyzed peat samples (yellow circles) obtained by subtracting the estimated MAAT  
1111 using the MBT<sub>5me</sub>' Deming calibration from the observed MAAT. (For interpretation  
1112 of the references to color in this figure legend, the reader is referred to the web  
1113 version of this article).

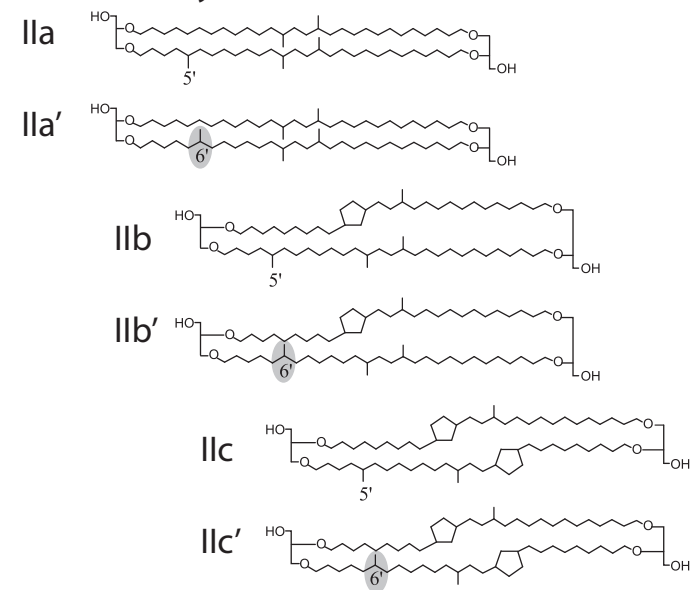
Table 1

Depth (cm)	Age (yr)	MBT <sub>5ME'</sub>	MAT <sub>mr</sub> soil (RMSE 4.6 °C)	MAT <sub>5me'</sub> soil (RMSE 4.8 °C)	MAAT <sub>peat</sub> (RMSE 4.7°C)
			De Jonge, 2014	De Jonge, 2014	This study
86	~700	0.53	6.6	10.9	4.5
102	~1000	0.53	6.6	11.3	4.8
838	~15,100	0.46	4.4	6.7	1.2
846	~15,400	0.39	2.8	5.4	-2.7
		<b>Δ MAAT</b>	<b>3.0 °C</b>	<b>5.0 °C</b>	<b>5.4 °C</b>

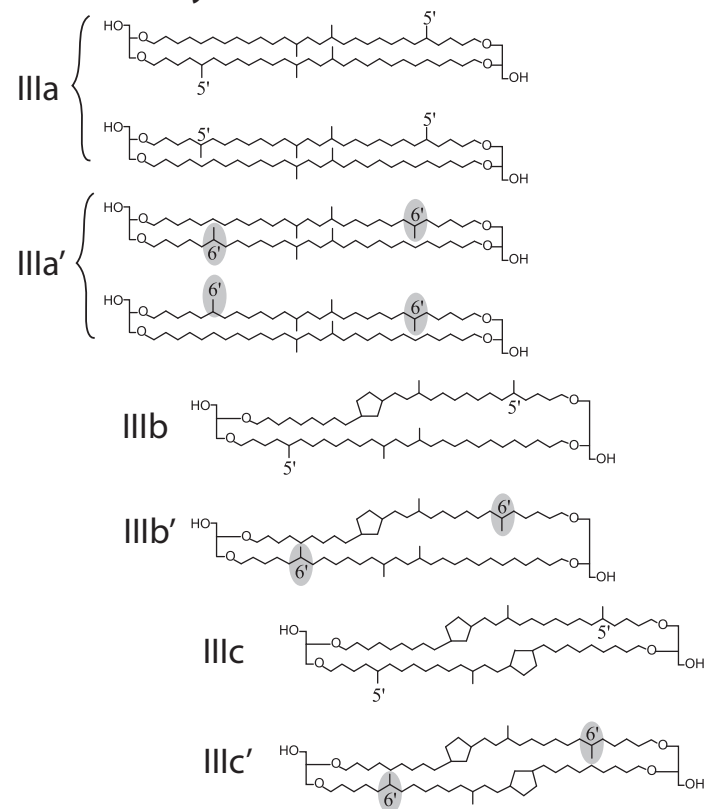
## Figure 1 Tetramethylated brGDGTs



## Pentamethylated brGDGTs



## Hexamethylated brGDGTs



## Crenarchaeol

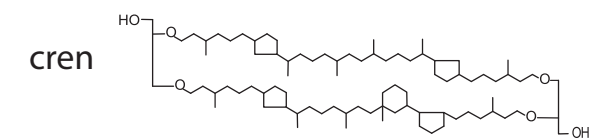


Figure 2

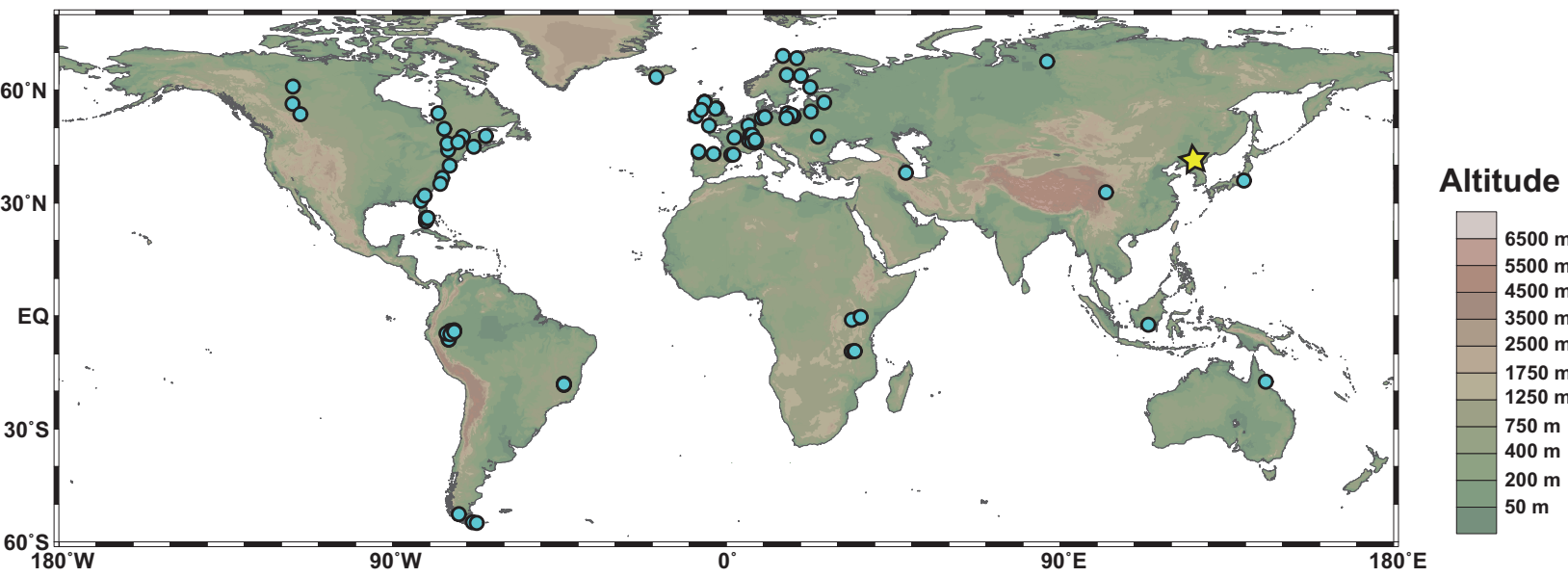


Figure 3

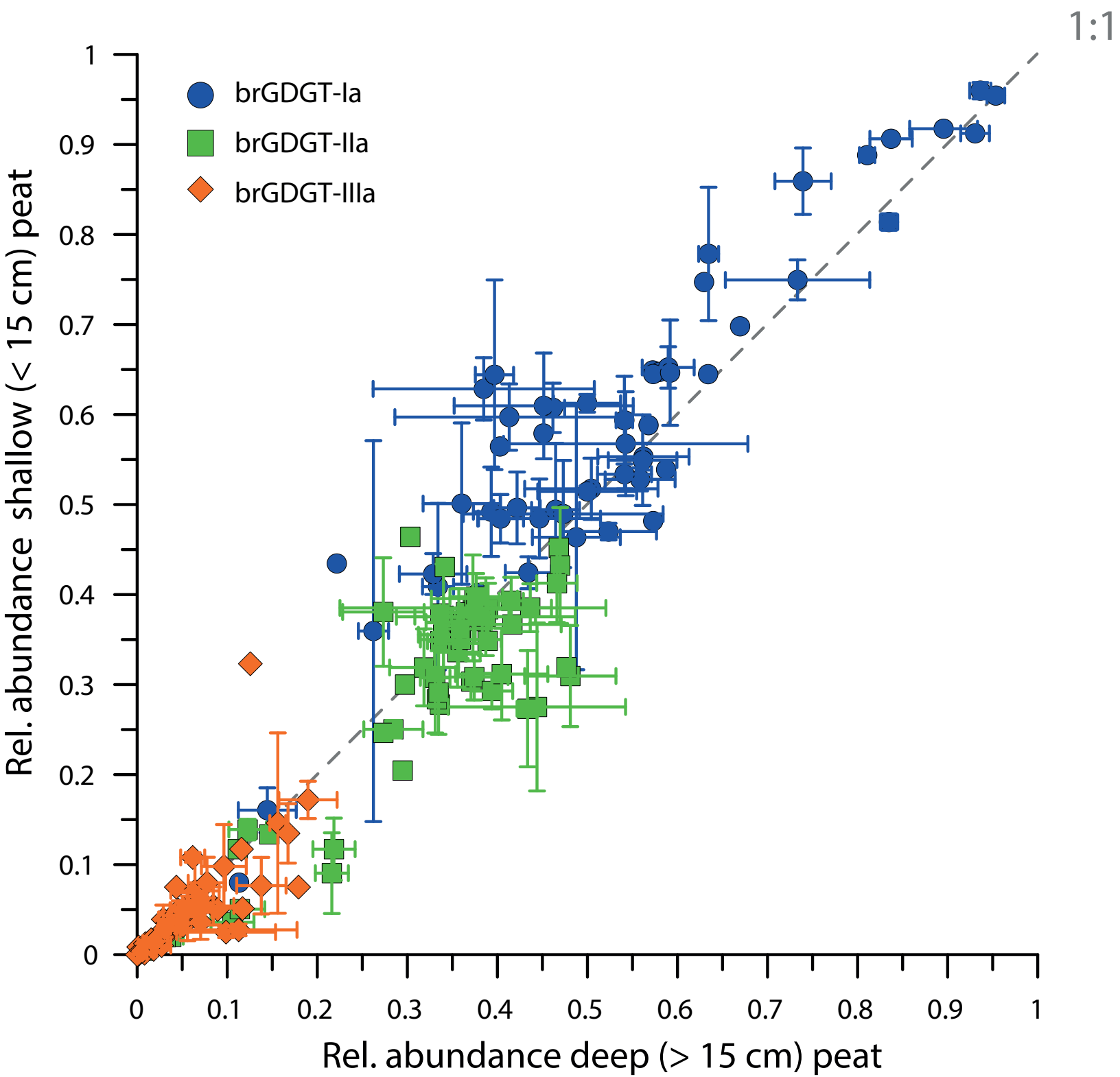


Figure 4

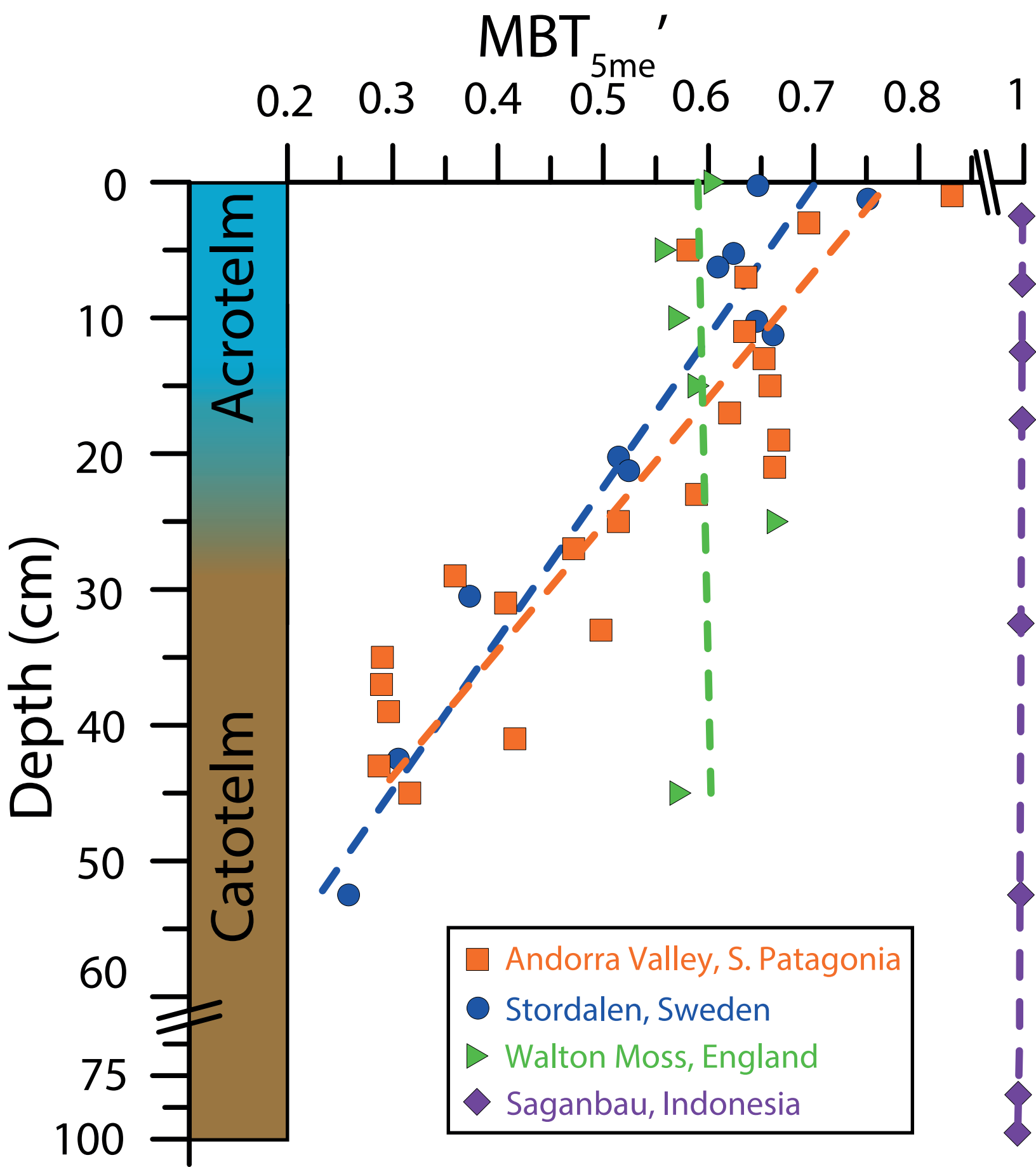




Figure 6

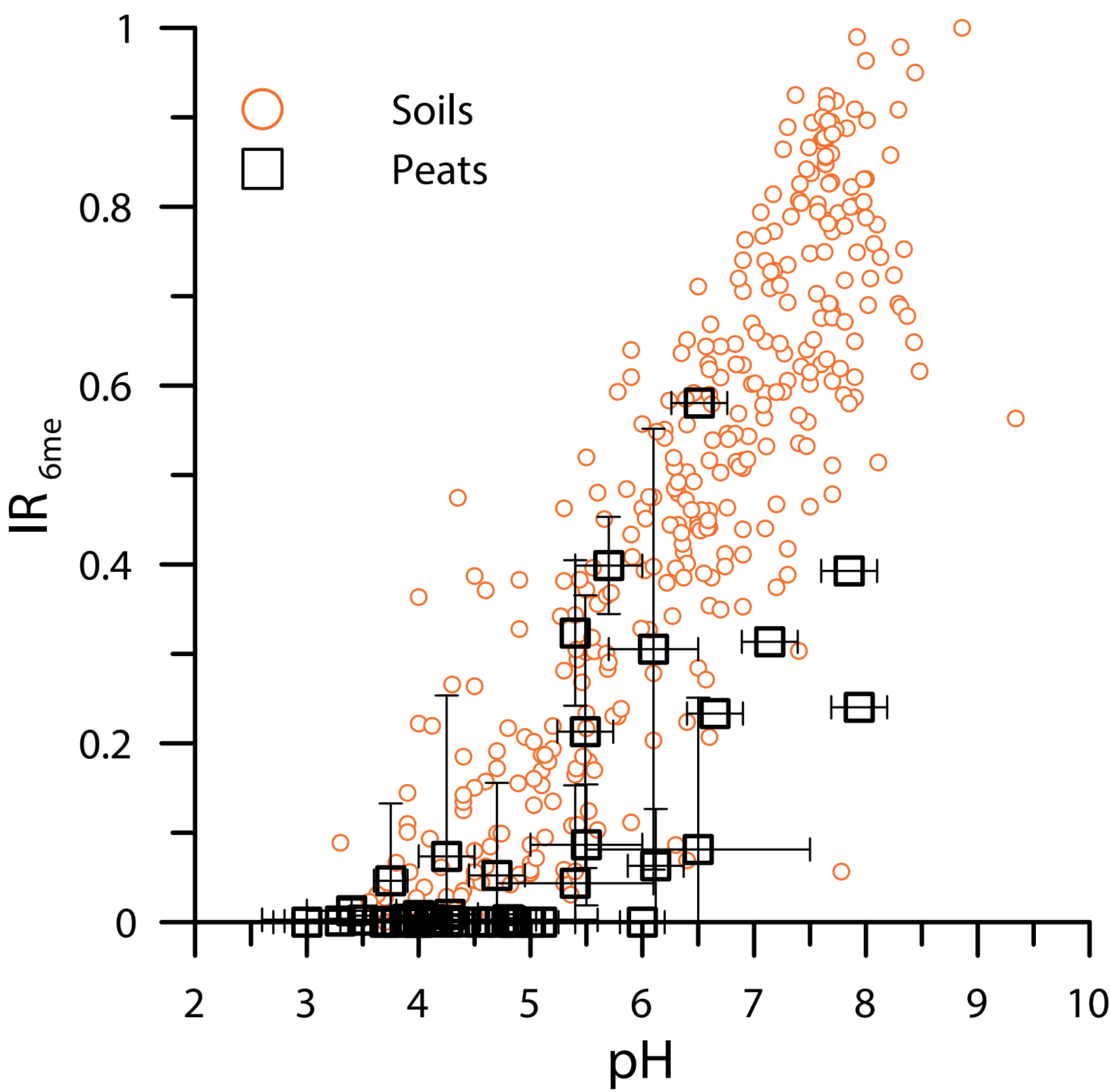


Figure 7

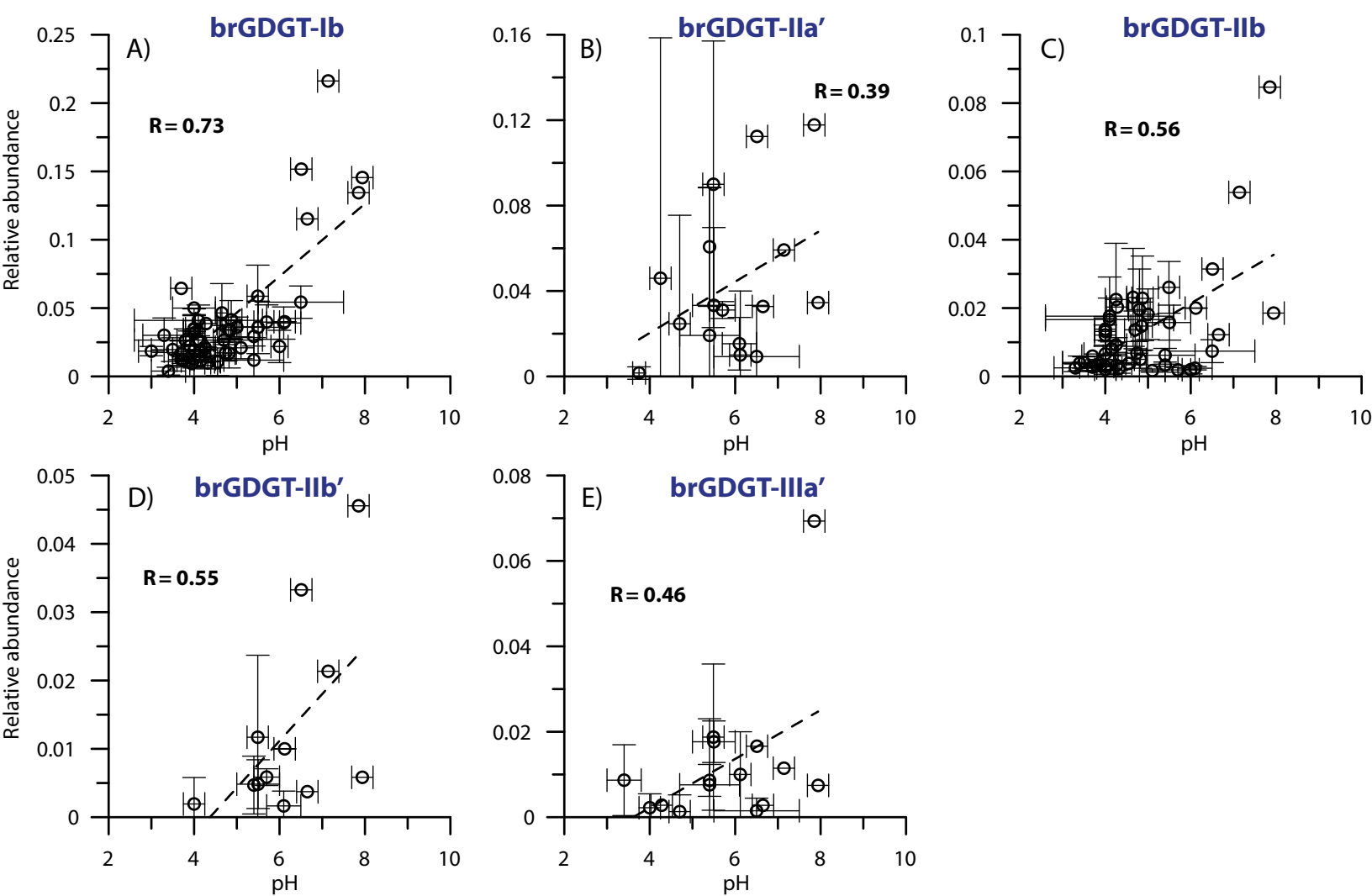


Figure 8

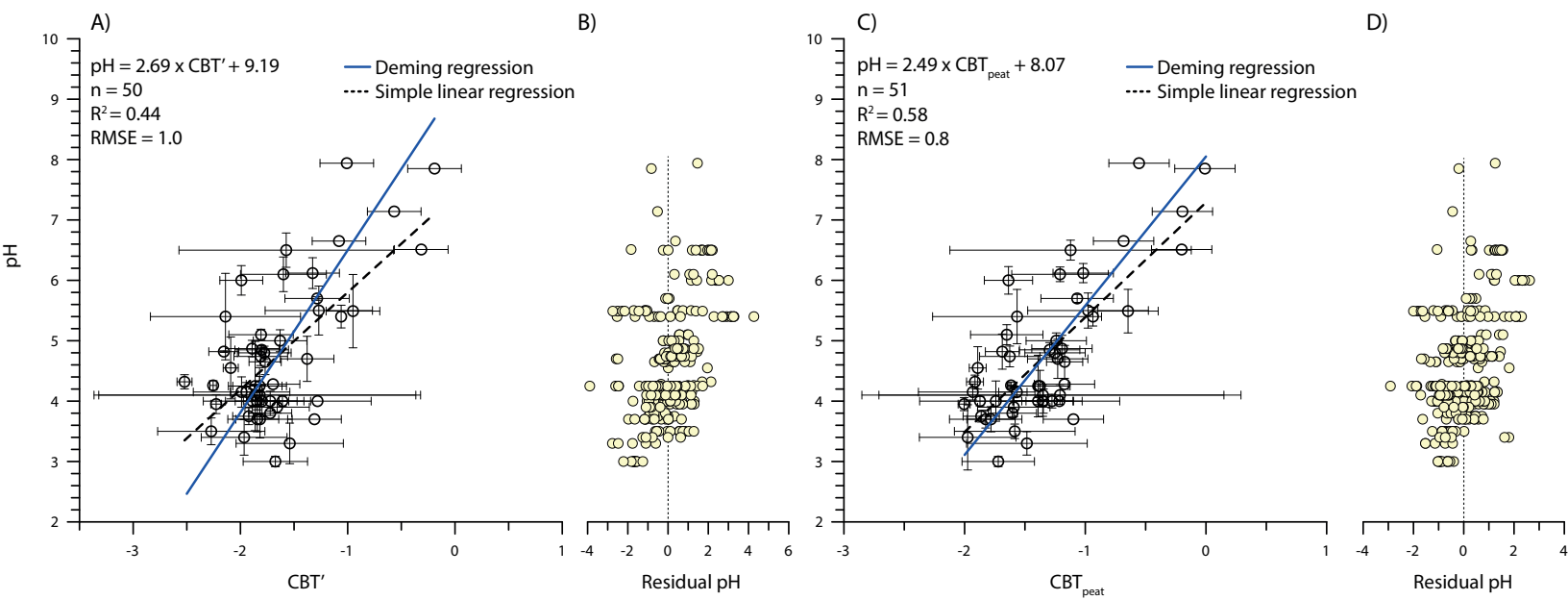


Figure 9

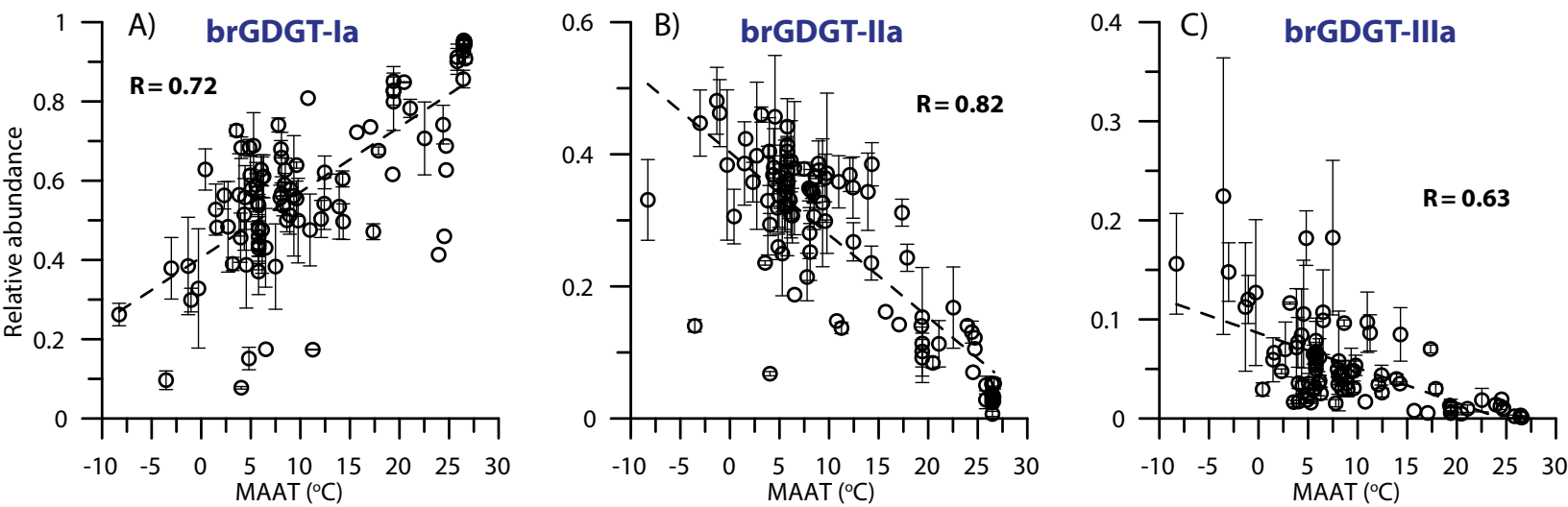


Figure 10

